

Cavity Optomechanics in the Single-photon
Strong Coupling Regime

單光子強耦合領域中的腔光力學

XU, Gaofeng

徐高峰

A Thesis Submitted in Partial Fulfillment
of the Requirements for the Degree of
Master of Philosophy
in
Physics

The Chinese University of Hong Kong
September 2013

Abstract

We investigate theoretically the quantum effects of optomechanical couplings between a single-mode cavity field and a mechanical oscillator in the single-photon strong coupling regime. In such a regime, we examine a driven optomechanical system and derive a two-level model under certain conditions. Such a model gives rise to a scheme of generating a single photon in the cavity, which is verified by numerical calculations based on the Schrödinger equation. For an optomechanical cavity driven by two lasers, we discover a class of dark states that are eigenvectors of the Hamiltonian of the driven optomechanical system. Such dark states leads to the decoupling of the cavity field from the external driving, which is analogous to coherent population trapping (CPT) in atomic physics. In addition, we demonstrate with numerical simulation based on the master equation that these dark states can be prepared with high fidelities by optical pumping. For a driven optomechanical cavity with a two-level atom inside, we achieve an effective coupling between the atom and mechanical oscillator, which is mediated by the cavity field. Such an effective coupling leads to a Rabi oscillation in which the excitation of the atom is accompanied by the excitation of a phonon. Specifically, we observe these Rabi oscillations and quantify the effects of dissipations in numerical simulations.

摘要

我們從理論上探究在單光子強耦合領域中一個單模腔場與一個力學振子的光力學耦合的量子效應。在該領域，我們考察一個被驅動的光力學系統並在一定條件下匯出一個二能級模型。這個模型引出了一個在腔中生成一個單光子的方案，而此方案得到了基於薛定諤方程的數值計算的確認。對於一個受到兩束鐳射驅動的光力學系統，我們發現了一類暗態，這些暗態是系統哈密頓量的本征態。這些暗態導致腔場與外界驅動場之間去耦合，而這是原子物理學中相干布居囚禁的類推。另外，我們用基於主方程的數值模擬展示了可以通過光泵浦製備出具有高保真度的暗態。對於一個腔內有一個二能級原子的受驅動光力學系統，我們獲得了由腔場媒介的原子與力學振子的有效耦合。這種有效耦合展現出拉比振盪，其中原子的激發伴隨著一個聲子的激發。確切地，我們在數值模擬中觀察到了這些拉比振盪並量化了耗散的效應。

ACKNOWLEDGMENTS

First of all, I thank my supervisor Prof. Law for leading me all the way here to present people this thesis. I still remember how I learn knowledge little by little from a student who knows almost nothing about research. It is Prof. Law who has made the my two years study in CUHK so rewarding.

I also thank Prof. Zhou and Prof. Liu, for their kind help with my application for PhD and for teaching me the courses quantum mechanics and statistical mechanics. There are many enlightening moments in the classes, which I enjoyed a lot. Besides, I thank Prof. Zhu for being so nice to me, and for taking us to play basketball every Friday afternoon, which is actually my favorite activity in CUHK.

Particularly, I thank Dr. Liao Jieqiao, former postdoctoral fellow of our group, for teaching me a lot of things. Dr. Liao's kind help made it much easier for me to start my research works. I am also grateful to Dr. Wei Bobo, Mr. Xie Yichao, Dr. Chu Zhiqin and Dr. Chen Shaowen, whose guidance are so important to me.

Last but not least, I thank my peers, who made my life so much fun. I cannot imagine how my life will be like without you guys. Your names are not listed here, but definitely in my heart always.

Thank you all! I wish you all the best!

Contents

1	Introduction	1
2	Basic Description of Optomechanical Systems	4
2.1	The Physical System: Basic Components	4
2.2	Hamiltonian Model	6
2.3	Energy-level Structure	8
2.4	Weak Coupling Regime: Linearized Theory	10
2.5	Single-photon Strong Coupling Regime	13
2.6	Damping of the System	17
3	Single-photon Generation in a Cavity via an Optomechanical Resonance	20
3.1	Introduction	20
3.2	Two-level Model	22
3.3	Rabi Oscillations in an Ideal Cavity	26
3.4	Numerical Results	27
3.5	Effects of Cavity Field Damping	31
3.6	Connection to Photon Blockade Effect	33
3.7	Conclusion	36
4	Optomechanical Dark States	37
4.1	Introduction	37

4.2	Review of Dark States in Three-level Systems	38
4.3	The Model	40
4.4	Effective Hamiltonian in a Confined Hilbert Space	42
4.4.1	Resonant Hamiltonian under RWA	42
4.4.2	Truncation of Hilbert Space by Using $g = g_N$	44
4.5	Dark States	46
4.6	Preparation of Dark States by Optical Pumping	50
4.7	Conclusion	55
5	Optomechanical Cavity with an Atom: an Effective Atom-mirror	
	Coupling	57
5.1	Introduction	57
5.2	The Model	58
5.3	Effective Two-level Hamiltonian	60
5.4	Improvement of the Two-level Model	64
5.5	Atom-mirror Rabi Oscillations	66
5.6	Effects of Damping	70
5.7	Conclusion	74
6	Conclusion	75

List of Figures

2.1	Schematic diagram of an optomechanical system consisting of a Fabry-Perot cavity with one harmonically bounded mirror. . . .	5
2.2	The energy-level structure of the optomechanical system up to two-photon subspaces. We define $\delta = -g^2/\omega_M$ for convenience. . . .	10
2.3	Comparison between the linearized theory (red lines) and the exact quantum equations (blue lines) in cavity photon numbers $\langle a^\dagger a \rangle$ and phonon numbers $\langle b^\dagger b \rangle$. Common parameters: $\Delta/\omega_m = 1.01$, $\Omega/\omega_m = 0.2$. Tuned parameter: (a) and (b): $g/\omega_m = 0.1$; (c) and (d): $g/\omega_m = 0.2$; (e) and (f): $g/\omega_m = 0.3$	15
3.1	Energy-level diagram of an optomechanical system with a laser driving (green arrays) for illustrating photon blockade effect. Here the parameter $\delta = g^2/\omega_M$	21
3.2	Schematic diagram of the two-level model of a driven optomechanical system ($\delta = g^2/\omega_M$).	23
3.3	Time evolution of single-photon probability. Parameters are set as: $g/\omega_M = 0.5$, $\Delta_0/\omega_M = -0.75$; (a) $\Omega/\omega_M = 0.05$; (b) $\Omega/\omega_M = 0.1$; (c) $\Omega/\omega_M = 0.2$	28
3.4	Compare of T_0 between analytical result of the model (lines) and numerical calculations (dots). Parameters are set as: (a) Red line: $g/\omega_M = 0.5$, Blue line: $g/\omega_M = 0.3$; (b) Green line: $\Omega/\omega_M = 0.1$, blue line: $\Omega/\omega_M = 0.05$, red line: $\Omega/\omega_M = 0.01$	30

3.5	Maximal probability of the single-photon state P_{max} as a function of off-resonance detuning $\tilde{\Delta}$. Parameters are set as: square: $g/\omega_M = 0.5$, $\Omega/\omega_M = 0.1$; circle: $g/\omega_M = 0.7$, $\Omega/\omega_M = 0.05$	31
3.6	Evolution of the single-photon state probability P for different decay rates in a pulse-driving optomechanical system. Parameters are set as: $g/\omega_M = 0.55$, $\Omega/\omega_M = 0.055 \cdot \theta(T_0 - t)$, where $\theta(T_0 - t)$ is a step function and $T_0 = 34\omega_M^{-1}$	33
3.7	Evolutions of (a) average photon numbers and (b) two-photon equal time correlation function $g^{(2)}(0)$. The green line in (a) is the total number of photons in the cavity, while the blue one is the number only takes into account photons in single-photon states. Parameters are set as: $g/\omega_M = 0.50$, $\Omega/\omega_M = 0.05$, $\Delta/\omega_M = 0.25$, $\kappa/\omega_M = 0.05$	35
4.1	Energy-level diagram of a Λ -type three-level atom driven by two near-resonant lasers.	39
4.2	Schematic diagram of an optomechanical system consisting of a fixed end mirror and a movable end mirror with two driving fields.	41
4.3	The coupling scheme between energy levels of the optomechanical system (only zero- and one-photon states are shown). Here each laser is used to establish a set of resonant transitions, and $ p\rangle_M = \tilde{p}(0)\rangle_M$ and $ \tilde{p}\rangle_M = \tilde{p}(1)\rangle_M$ for simplicity. By choosing $g = g_N$, there is no transition between $ 0\rangle_c N\rangle_M$ and $ 1\rangle_c \tilde{N}\rangle_M$	43
4.4	Exact solution of g_N satisfying Eq. (4.17) as a function of N (points) and result of asymptotic behavior based on Eq. (4.18)(solid line).	45
4.5	Exact solution of g_N satisfying Eq. (4.17) as a function of N (points) and result of asymptotic behavior based on Eq. (4.18)(solid line).	46

- 4.6 Evolution of fidelity $F = |\langle D(t)|\Psi(t)\rangle|^2$ with initial state set as a dark state. The $|\Psi(t)\rangle$ is the numerical solution of the Schrödinger equation defined by the Hamiltonian H_r . The parameters are: $g/\omega_M = 0.37$, $\Omega_1/\omega_M = 0.01$, $\Omega_2/\omega_M = 0.03$, $\Delta_1/\omega_M = -0.14$, $\Delta_2/\omega_M = -1.14$ 47
- 4.7 An illustration of some phonon statistics of dark states. (a) Phonon number probability distribution $P_m = |C\beta_m|^2$ of dark states for different ratios of driving strengths, with $g_N = 0.37\omega_M$ and $N = 10$. (b) $\langle(\Delta n)^2\rangle/\langle n\rangle$ as a function of Ω_1/Ω_2 for $g/\omega_M = 0.17, 0.64, 0.76$ corresponding to $N = 20, 3, 2$ respectively. 49
- 4.8 Preparation of dark states by optical pumping. The fidelities F for various Ω_2/Ω_1 ratios are plotted as a function of time. The parameters are: $g_N/\omega_M = 0.37$, $N = 10$, $\kappa/\omega_M = 0.05$, $\Omega_2/\omega_M = 0.01$, $\Delta_1/\omega_M = -0.14$, $\Delta_2/\omega_M = -1.14$ 52
- 4.9 Time evolution of the fidelities F for various g in the vicinity of $g_N = 0.37\omega_M$. The parameters are: $\kappa/\omega_M = 0.05$, $\Omega_1 = \Omega_2 = 0.01\omega_M$, $\Delta_1/\omega_M = -0.14$, $\Delta_2/\omega_M = -1.14$ 53
- 4.10 Evolution of fidelity F for a mechanical damping rate $\gamma_M/\omega_M = 5 \times 10^{-5}$ and thermal phonon number $\bar{n}_M = 0$. The inset figure shows the final fidelity F_f (at $\omega_M t = 10^4$) for various γ_M , with thermal phonon numbers are $\bar{n}_M = 0$ (red squares) and $\bar{n}_M = 1$ (blue circles). The parameters are: $g/\omega_M = 0.37$, $\kappa/\omega_M = 0.05$, $\Omega_1 = \Omega_2 = 0.01\omega_M$, $\Delta_1/\omega_M = -0.14$, $\Delta_2/\omega_M = -1.14$ 54
- 5.1 Schematic diagram of an optomechanical system with a two-level atom inside, driven by an external field. 59
- 5.2 (a) Energy-level structure of the atom assisted optomechanical system, driven by an external field. (b) Scheme of the Λ type three-level model under the large detuning and resonance conditions. 61

5.3	The product of Franck-Condon factors $A_{0,0}A_{1,0}$ as a function of g/ω_M	64
5.4	Evolution of the probability P of the system being in the state $ e\rangle 1\rangle_M \otimes 0\rangle_C$, for different detuning Δ_2 . Other parameters are: $\Delta_3 = 0$, $g = 0.4\omega_M$, $\Omega = G = 0.05\omega_M$	68
5.5	Evolution of the probability P of the system being in the state $ e\rangle 1\rangle_M \otimes 0\rangle_C$ based on the numerical simulations (blue lines), the primary model (green dashed lines) and the improved model (red lines). The parameters are: (a) $\Delta_2 = 0.4\omega_M$, (b) $\Delta_2 = 0.6\omega_M$; with the other parameters: $\Delta_3 = 0$, $g = 0.4\omega_M$, $\Omega = G = 0.05\omega_M$	69
5.6	Dependence of the maximal probability P_m on Δ_3 . Other parameters are: $g = 0.4\omega_M$, $\Omega = G = 0.05\omega_M$	70
5.7	Damping effects of the atom (a), mechanical oscillator (b) and cavity field (c) on the atom-mirror Rabi oscillation. In each figure, the blue line is the probability of the system in the excited state $ g\rangle 0\rangle_M \otimes 0\rangle_C$, and red line is the total probability of being in the ground state $ g\rangle 0\rangle_M \otimes 0\rangle_C$ and the excited state $ e\rangle 1\rangle_M \otimes 0\rangle_C$. Other parameters are: $g = 0.4\omega_M$, $\Omega = G = 0.05\omega_M$, $\Delta_2 = 0.4\omega_M$	73

Chapter 1

Introduction

Cavity optomechanics is a thriving subject that studies the coupling between an optical field in a cavity and a mechanical oscillator via radiation pressure [1, 2, 3, 4, 5, 6]. The study of optomechanical coupling is mainly aimed at controlling quantum states of a macroscopic mechanical oscillator and its prospective applications in quantum information processing. For such a purpose, a number of proposals have been made, such as the storage of optical information as a mechanical excitation [7], quantum state transfer between light and macroscopic oscillators [8] and optomechanical transducers for long-distance quantum communications [9]. Besides, the study of optomechanics provides a route to fundamental tests of quantum mechanics in the macroscopic regime. Related studies include quantum entanglements [10, 11, 12, 13, 14, 15, 16, 17], Schrödinger cat states [18, 19, 20, 21], and the modification of uncertainty relations due to quantum gravity [22].

The study of cavity optomechanics dates back to late 1960s, when Braginsky investigated the effect of radiation pressure on a macroscopic harmonically bounded cavity mirror [23]. Starting from 1990s, this field goes into fast developing. An important achievement in this field is laser cooling of the mechanical oscillator to near its ground state, which lays the foundation for further control

of the quantum state of the mechanical oscillator. Besides, various schemes of high sensitive detections of mechanical motions have been developed [24, 25, 26]. Notably, an effect of optomechanically induced transparency has been proposed and experimentally demonstrated [27, 28, 29, 30, 31, 32, 33], which is an analogy of electromagnetically induced transparency (EIT) in atomic physics. Other achievements includes: optical spring effect [34], parametric instability [35], generating squeezed states of light [36] and mechanical oscillators [37, 38], etc.

In addition, cavity optomechanics is approaching the single-photon strong coupling regime, in which the radiation pressure of a single photon displaces the mechanical oscillator by a distance comparable to its zero-point fluctuation. In experiments, great progresses have been made in increasing single-photon optomechanical coupling strength [25, 39, 40, 41, 42, 43, 44, 45, 46]. In particular, in optomechanical system with a cloud of ultracold atoms as a mechanical oscillator, the single-photon strong coupling regime has already been reached [47]. A sufficiently strong single-photon optomechanical coupling strength is essential to the observation of the nonlinear quantum nature of optomechanical couplings. Remarkably, theorists have put forward a number of interesting phenomena in this regime of cavity optomechanics, such as photon blockade effect [48], generation of nonclassical states of the mechanical oscillator [49], multiple mechanical sidebands [50], and mechanical backaction effects on photon statistics [51]. Motivated by such trends, we devote this thesis to the study of interesting phenomena of optomechanical systems in this single-photon strong coupling regime.

The organization of the thesis is as follows. After a general introduction of cavity optomechanics in Chapter 1, we provide basic experimental setups and theoretical descriptions of optomechanical systems in Chapter 2. Then, in Chapter 3 we investigate the generation of a single cavity photon via an optomechanical resonance. In Chapter 4, we examine an optomechanical cavity driven by two lasers, and discover a class of dark states that is a superposition of mirror Fock

states. In these dark states, the cavity field is decoupled from the two driving lasers and remain in vacuum, which is an effect of quantum destructive interference. In Chapter 5, we study a composite system consisting of an optomechanical cavity and a two-level atom inside the cavity. In such a system, the cavity field is coupled to the mechanical oscillator and the atom separately. However, we find that an effective coupling between the atom and the mechanical oscillator can be achieved with the cavity field serving as a medium. Such an effective coupling exhibits Rabi oscillations involving atomic and mechanical states, which leads to a full atom-mirror entanglement and a quantum state transfer scheme between the atom and the mirror. Finally, we conclude the thesis in Chapter 6.

Chapter 2

Basic Description of Optomechanical Systems

In this chapter, we provide a background of cavity optomechanical systems. We first describe the basic settings and Hamiltonian models. Then, we review basic theoretical approaches in studying the quantum dynamics.

2.1 The Physical System: Basic Components

A generic cavity optomechanical system is formed by a Fabry-Perot cavity with a harmonically bounded cavity mirror, while the other mirror is fixed, as shown in Fig. 2.1. The resonant frequencies of electromagnetic fields inside the cavity are determined by the cavity length L . Generally, the frequency of the n -th cavity mode ω_n can be expressed as $\omega_n = \omega_n(L)$, where the function $\omega_n(L)$ is related to specific details of a cavity. In typical studies of optomechanics, we are interested in the situation where only a single cavity field mode is involved, since the separation of mode frequencies is set to be large enough to avoid exciting other modes when the cavity is driven by a laser at a frequency near resonant to the cavity mode of interest. In this thesis, we denote the frequency of the cavity

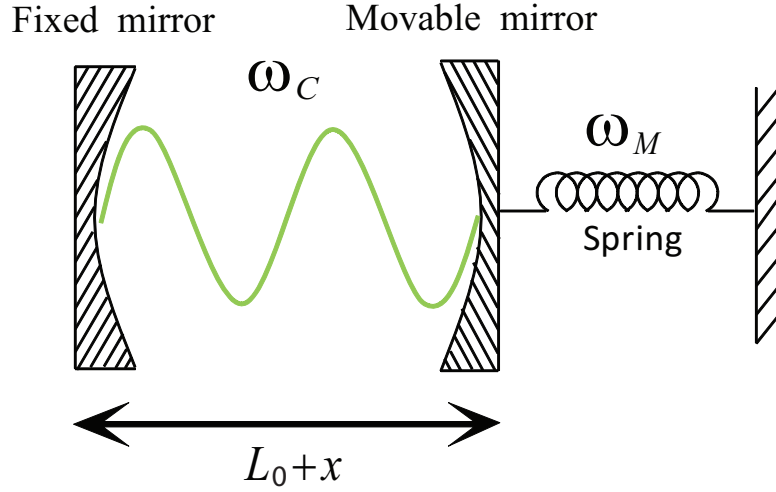


Figure 2.1: Schematic diagram of an optomechanical system consisting of a Fabry-Perot cavity with one harmonically bounded mirror.

field mode as ω_C . The length of the cavity typically is in the range of 10^{-2}m , but it can be as small as 10^{-5}m in a photonic crystal setup [6].

The harmonically bounded end mirror is regarded as a simple harmonic oscillator, with an oscillating frequency ω_M ranging from kHz [52] to GHz [40]. In experiments, the effective mass of the mechanical oscillator M spans a wide range of scales. For example, the mechanical oscillator can be a cloud of ultracold atoms with a mass as small as 10^{-22}kg [47]. On the other hand, a macroscopic suspended mirror in a gravitational wave detector has a mass in kilogram scale [53]. In typical experiments, the effective mass is around $M \sim 10^{-12}\text{kg}$ [46]. The mass and frequency of the oscillator determine an important length scale of the quantum system, namely zero-point fluctuation of the position:

$$x_{zpf} = \sqrt{\hbar/(2M\omega_M)}, \quad (2.1)$$

which shall be used in the derivation of optomechanical coupling in the following section.

In the optomechanical system depicted in Fig. 2.1, the cavity field and the movable mirror are coupled with each other via radiation pressure of the field on

the mirror. Such an interaction is characterized by the single-photon coupling strength g (to be defined in the next section), which ranges from 1Hz [54], to 10^6 Hz as realized in a photonic crystal cavity where the dimension of the cavity is of order $1\mu\text{m}$ and the mass of the mechanical oscillator is about 300fg, which are relatively small [40].

We remark that optomechanical couplings can be realized with a variety of configurations, not limited to the Fabry-Perot cavity [55]. In fact, experiments have been performed in other systems such as microtoroids with whispering gallery modes [57], waveguides and photonic crystal cavities [39], suspended membrane inside a cavity [24, 25, 58] and ultracold atoms in a cavity [47]. These different implementations share the same principle that a mechanical motion is forced by an optical field, and the frequency (energy) of the optical field is modulated by the mechanical motion, thus leading to an optomechanical coupling.

2.2 Hamiltonian Model

To study the quantum effects, we need to set up the Hamiltonian first. The Hamiltonian of a cavity optomechanical system under single-mode adiabatic approximation is given by

$$H = \hbar\omega_C a^\dagger a + \hbar\omega_M b^\dagger b, \quad (2.2)$$

where a (b) and a^\dagger (b^\dagger) are respectively the annihilation and creation operator the cavity field (mechanical) modes, with $\omega_C = \omega_C(L_0 + x)$ the frequency of the cavity mode when the cavity is at its length $L_0 + x$ (Fig. 2.1). The dependence of cavity field resonant frequency ω_C on mirror displacement x due to radiation pressure is the key to optomechanical coupling. We assume that the displacement of the mirror is much smaller than the wavelength of the cavity field mode, i.e., $x \ll \lambda$ (this condition automatically leads to $x \ll L_0$), therefore the frequency of

the cavity field mode with a cavity length $L_0 + x$ can be expanded as:

$$\omega_C(L_0 + x) \approx \omega_C(L_0) + \left. \frac{\partial \omega_C}{\partial x} \right|_{L_0} \cdot x, \quad (2.3)$$

where we have made a linear approximation by neglecting higher order corrections in the expansion since x is much smaller than L_0 . In addition, we assume that the mirror is moving adiabatically slow so that scattering of the cavity field mode to other modes are negligible. This requires the mirror frequency be much smaller than the frequency separations of neighboring cavity field modes. Under such conditions, the Hamiltonian of a single cavity field mode coupled to a moving mirror via radiation pressure is approximated by

$$\begin{aligned} H &= \hbar \omega_C(L_0 + x) a^\dagger a + \hbar \omega_M b^\dagger b \\ &\approx \hbar \omega_C(L_0) a^\dagger a + \hbar \frac{\partial \omega_C}{\partial x} x_{zpf} a^\dagger a (b + b^\dagger) + \hbar \omega_M b^\dagger b, \end{aligned} \quad (2.4)$$

where we have used the relation $x = x_{zpf} (b + b^\dagger)$. We emphasize that $\omega_C(L_0)$ in Eq. (2.4) is the frequency of the cavity mode at the rest length of the cavity. Thus, we identify the single-photon coupling strength

$$g = -\frac{\partial \omega_C}{\partial x} x_{zpf}, \quad (2.5)$$

which represents the modification of resonant frequency when the mirror is displaced by a distance of zero-point fluctuation, and the minus sign is added following the usual treatments. For a one dimensional Fabry-Perot cavity, we have approximately $\partial \omega_C / \partial x \approx -\omega_C / L_0$, therefore the single-photon coupling strength reads

$$g \approx \frac{x_{zpf}}{L_0} \omega_C. \quad (2.6)$$

To summarize, after making the linear and adiabatic approximation which is valid under the conditions of small mirror displacement and slow mirror motion, we achieve the Hamiltonian of an cavity optomechanical system:

$$H = \hbar \omega_C a^\dagger a - \hbar g a^\dagger a (b + b^\dagger) + \hbar \omega_M b^\dagger b, \quad (2.7)$$

in which we see the field-mirror interaction ($-\hbar g a^\dagger a (b + b^\dagger)$) involves products of three operators, showing the nonlinear nature of the interaction. Alternatively, the Hamiltonian (2.7) can be expressed with the position x and momentum p of the mechanical oscillator as:

$$H = \hbar\omega_C a^\dagger a - \hbar g a^\dagger a \frac{1}{x_{zpf}} x + \frac{1}{2M} p^2 + \frac{1}{2} M \omega_M^2 x^2. \quad (2.8)$$

Here the term $-\hbar g a^\dagger a \frac{1}{x_{zpf}} x$ stands for the potential energy due to radiation pressure, from which we see the radiation pressure force is

$$F = \hbar \frac{g}{x_{zpf}} a^\dagger a, \quad (2.9)$$

which is proportional to coupling strength and photon number.

We note that a rigorous formulation of the Hamiltonian without single-mode adiabatic approximation is provided by Ref. [59]. We also remark that in some schemes the modulation of cavity frequency by the mirror position can be nonlinear [24, 25, 58]. For example, cavity frequency can be modulated as: $\omega(L_0 + x) - \omega(L_0) \propto x^2$, which has been realized in an optomechanical cavity with a membrane inside [25]. In Ref. [25], it is reported that by positioning the membrane at a node or antinode of the cavity wave, the linear dependence term can be turned off, i.e., $\partial\omega_C/\partial x = 0$, such that the second order term becomes dominant.

2.3 Energy-level Structure

In this section, we discuss the energy levels of the Hamiltonian of an optomechanical system. In a displaced picture defined by a displacement operator:

$$D(a^\dagger a g / \omega_M) = \exp\left[g \frac{a^\dagger a}{\omega_m} (b^\dagger - b)\right], \quad (2.10)$$

the Hamiltonian in Eq. (2.7) can be diagonalized as:

$$\tilde{H} = D^\dagger H D = \hbar\omega_C a^\dagger a + \hbar\omega_M b^\dagger b - \hbar \frac{g^2}{\omega_M} (a^\dagger a)^2, \quad (2.11)$$

which represents two decoupled quantum harmonic oscillators. Therefore, the eigenvectors of \tilde{H} in the displaced picture are products of Fock states of the cavity field and mirror: $|n\rangle_C \otimes |p\rangle_M$, where $n(p)$ is the cavity photon (phonon) number. The corresponding energy eigenvalues are:

$$\varepsilon_{n,p} = n\omega_C + p\omega_M - n^2g^2/\omega_M, \quad (2.12)$$

which depend nonlinearly on photon number n , and linearly on phonon number p . Here we have set $\hbar = 1$, and we will always use this convention for simplicity hereafter. Equivalently, the eigenvectors in the undisplaced picture are given by

$$|\psi_{n,p}\rangle = D(a^\dagger ag/\omega_M) |n\rangle_C \otimes |p\rangle_M = |n\rangle_C \otimes D(ng/\omega_M) |p\rangle_M = |n\rangle_C \otimes |\tilde{p}(n)\rangle_M, \quad (2.13)$$

where $|\tilde{p}(n)\rangle_M$ denotes the n -photon displaced Fock state of the mirror. Thus, the Hamiltonian can be expressed in the eigenbasis as:

$$H = \sum_{n,p} \varepsilon_{n,p} |\psi_{n,p}\rangle \langle \psi_{n,p}|, \quad (2.14)$$

which will be used in later studies.

The whole Hilbert space is divided into many subspaces, labeled by photon numbers. A part of the energy-level structure is illustrated in Fig. 2.2. The energy levels represent the eigenvectors $\psi_{n,p}$ for phonon number $n = 0, 1, 2$. In the states of an n -photon subspace, the cavity field is in n -photon Fock state $|n\rangle_C$, while the mirror is in n -photon displaced Fock state $|\tilde{p}(n)\rangle_M$, as are shown in the figure. Moreover, the energy levels inside each subspace are equally spaced, with a common separation ω_M . However, there is a nonlinear energy shift $-n^2g^2/\omega_M$ of each state due to the optomechanical coupling. As a result, energy levels between corresponding neighboring subspaces are not equally spaced. In Fig. 2.2, we only show the lowest three subspaces since the energy-level structures of subspaces with more photons are similar.

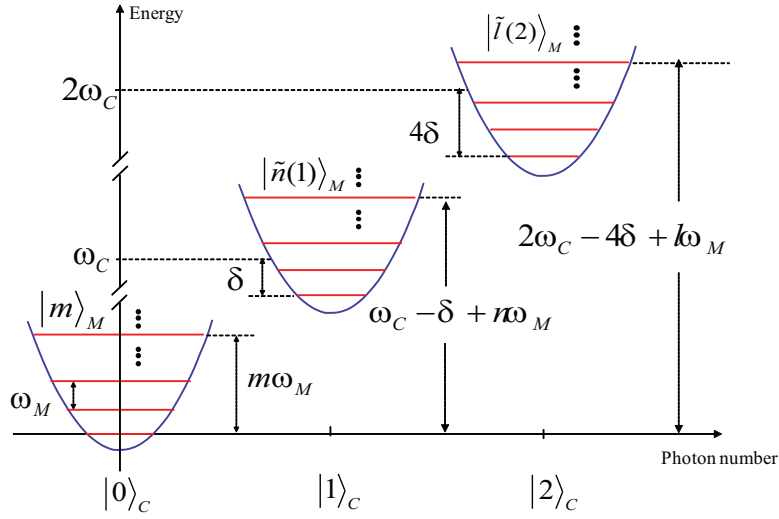


Figure 2.2: The energy-level structure of the optomechanical system up to two-photon subspaces. We define $\delta = -g^2/\omega_M$ for convenience.

2.4 Weak Coupling Regime: Linearized Theory

We now introduce a linearized theory of cavity optomechanics [62], which works in the weak optomechanical coupling regime: $g \ll \omega_M$. This theory is based on the assumption that the fluctuation of cavity field amplitude is much smaller than its average.

We consider a driven optomechanical system, whose Hamiltonian is given by:

$$H = \omega_c a^\dagger a + \omega_m b^\dagger b - g a^\dagger a (b^\dagger + b) + \Omega e^{-i\omega_L t} a^\dagger + \Omega^* e^{i\omega_L t} a, \quad (2.15)$$

where the term $\Omega e^{-i\omega_L t} a^\dagger + \Omega^* e^{i\omega_L t} a$ describes that the cavity photons are driven by a laser with an amplitude Ω and a frequency ω_L . To eliminate the time-dependence in this Hamiltonian, we go to a rotating frame with a transformation operator: $T_1(t) = e^{-i\omega_L a^\dagger a t}$. Consequently, the transformed Hamiltonian ($H' = T_1^\dagger H T_1 - i T_1^\dagger \dot{T}_1$) reads

$$H' = \Delta a^\dagger a + \omega_m b^\dagger b - g a^\dagger a (b^\dagger + b) + \Omega a^\dagger + \Omega^* a, \quad (2.16)$$

where the laser detuning $\Delta = \omega_c - \omega_L$ is defined. Therefore, we obtain the

Heisenberg's equations of motion of a and b :

$$\begin{cases} \dot{a} = -i\Delta a + ig a(b^\dagger + b) - i\Omega, \\ \dot{b} = -i\omega_m b + ig a^\dagger a. \end{cases} \quad (2.17)$$

In the linearized theory, we separate the operators into two parts: a c-number part that accounts for the average and the operator part that reveals the quantum fluctuation. Specifically, we decompose the operators as:

$$\begin{cases} a(t) = \alpha(t) + \delta a(t), \\ b(t) = \beta(t) + \delta b(t), \end{cases} \quad (2.18)$$

where $\alpha(t) = \langle a(t) \rangle$ ($\beta(t) = \langle b(t) \rangle$) is a c number that describes the expectation value of $a(t)$ ($b(t)$), while $\delta a(t)$ and $\delta b(t)$ are operators that take care of the quantum fluctuations upon the averages. Substituting Eq. (2.18) into the Heisenberg's equations (2.17), we obtain the (classical) equations for the mean values:

$$\begin{cases} \dot{\alpha}(t) = -i\Delta\alpha + ig(\beta + \beta^*)\alpha - i\Omega, \\ \dot{\beta}(t) = -i\omega_m\beta + ig|\alpha|^2, \end{cases} \quad (2.19)$$

and the operator equations for the quantum fluctuation are given by

$$\begin{cases} \frac{d}{dt}\delta a(t) = -i[\Delta - g(\beta + \beta^*)]\delta a + ig\alpha(\delta b^\dagger + \delta b) + ig\delta a(\delta b^\dagger + \delta b), \\ \frac{d}{dt}\delta b(t) = -i\omega_m\delta b + ig(\alpha^*\delta a + \alpha\delta a^\dagger) + ig\delta a^\dagger\delta a. \end{cases} \quad (2.20)$$

We can view the operator equations (2.20) as Heisenberg's equations of motion for δa and δb in a new Hamiltonian, i.e., the effective Hamiltonian for δa and δb .

Such an effective Hamiltonian takes the form:

$$\begin{aligned} H_{eff} = & [\Delta - g(\beta + \beta^*)]\delta a^\dagger\delta a + \omega_m\delta b^\dagger\delta b - g\delta a^\dagger\delta a(\delta b^\dagger + \delta b) \\ & - g(\alpha^*\delta a + \alpha\delta a^\dagger)(\delta b^\dagger + \delta b). \end{aligned} \quad (2.21)$$

We can take a linear approximation to neglect the nonlinear term $-g\delta a^\dagger\delta a(\delta b^\dagger + \delta b)$ in the Hamiltonian (2.21) under condition that

$$|\alpha|^2 \gg \langle \delta a^\dagger\delta a \rangle. \quad (2.22)$$

Therefore, the effective Hamiltonian in linear approximation becomes

$$H_{eff} \approx [\Delta - g(\beta + \beta^*)] \delta a^\dagger \delta a + \omega_m \delta b^\dagger \delta b - g(\alpha^* \delta a + \alpha \delta a^\dagger) (\delta b^\dagger + \delta b), \quad (2.23)$$

which can be interpreted as two linearly coupled oscillators. As a result, the linearized equations of motion for the fluctuations reads

$$\begin{cases} \frac{d}{dt} \delta a(t) = -i[\Delta - g(\beta + \beta^*)] \delta a + ig\alpha (\delta b^\dagger + \delta b), \\ \frac{d}{dt} \delta b(t) = -i\omega_m \delta b + ig(\alpha^* \delta a + \alpha \delta a^\dagger). \end{cases} \quad (2.24)$$

Thus, by solving mean value equation (2.19) and linearized fluctuation equation (2.24), the evolution of field operator can be obtained approximately.

The linearized theory has been applied to study various phenomena in cavity optomechanics. In particular, three types of interaction schemes can be realized corresponding to separate detunings of laser driving [6, 4]. First, when $\Delta = \omega_C - \omega_L \approx \omega_M$, i.e., the laser driving is red-detuned by about one mechanical frequency, we have two harmonic oscillators of similar frequencies coupled with each other according to the effective Hamiltonian [Eq. (2.23)]. Thus, the resonant interaction terms under rotating wave approximation is: $-g(\alpha^* \delta a \delta b^\dagger + \alpha \delta a^\dagger \delta b)$. Such an interaction allows energy exchange between the two harmonic oscillators, which has been used to achieve cooling of the mechanical excitations down to near its ground state [63, 64]. In the second scheme, we set $\Delta \approx -\omega_M$, which means that the laser driving is blue-detuned by about one mechanical frequency. For this case, the resonant interaction under rotating wave approximation is: $-g(\alpha^* \delta a^\dagger \delta b^\dagger + \alpha \delta a \delta b)$, which leads to "two-mode squeezing". This is the key to parametric amplification [65], in which energies of both the cavity field and mechanical oscillator grows exponentially in the absence of dampings. Third, when $\Delta \approx 0$, we have the interaction $-g(\alpha^* \delta a + \alpha \delta a^\dagger) (\delta b^\dagger + \delta b)$. Such an optomechanical coupling results in a phase shift of the cavity field proportional to the position of mechanical oscillator. By measuring this phase shift, the motion of the mechanical oscillator can be detected (optomechanical displacement detection)

[26]. Besides, an interesting phenomenon called optomechanically induced transparency has been discovered using the linearized theory [27, 30], which is analogous to the electromagnetically induced transparency (EIT) in atomic physics. In summary, the linearized theory has been proven to be successful in the weak coupling regime. However, the linearized theory is not sufficient in describing systems with a single-photon coupling strength comparable to mechanical frequency, i.e., the linearization condition (2.22) breaks down when $g \sim \omega_M$, which is going to be discussed in the following section.

2.5 Single-photon Strong Coupling Regime

In this section, we introduce the single-photon strong coupling regime, in which the radiation pressure of a single photon displaces the mirror to a distance comparable to its zero-point fluctuation. Explicitly, the displacement of mirror equilibrium position by a single photon can be evaluated by considering the new potential of the mirror, which consists of the original harmonic bounding and radiation pressure of a photon. According to Eq. (2.8), the potential of the mirror is:

$$V(x) = \frac{1}{2}M\omega_M^2x^2 - \frac{g}{x_{zpf}}x, \quad (2.25)$$

where we have let $\langle a^\dagger a \rangle = 1$ for a single photon radiation pressure. Consequently, the new equilibrium position of the mirror can be obtained:

$$x' = 2\frac{g}{\omega_M}x_{zpf}, \quad (2.26)$$

which is proportional to the single-photon coupling strength g . Therefore, the single-photon strong coupling regime is characterized by a single-photon coupling strength comparable to the mechanical frequency, i.e., $g \sim \omega_M$. In such a regime, the nonlinear optomechanical coupling becomes significant so that the linearized theory described in the previous section is inadequate [56]. However, various

interesting phenomena have been proposed in this regime, such as the photon blockade effect [48], non-Gaussian mechanical steady states [50], and statistical features of transmitted photons [51]. In addition, experimentalists have also been pursuing this regime with different configurations of optomechanical systems [40, 46, 39, 25, 41, 42, 43, 44, 45]. In this thesis, we will focus on phenomena in this regime without exploiting the linearized theory.

Before going into specific studies, we first indicate the limitations of the linearized theory by a comparison between results of the linearized theory and exact numerical solution of Schrödinger equation. In Eq. (2.16), we have obtained the Hamiltonian of a driven optomechanical system in a rotating frame. Numerically we solve the Schrödinger equation governed by this Hamiltonian

$$i\dot{|\Psi(t)\rangle} = H' |\Psi(t)\rangle, \quad (2.27)$$

with the state of the system in the form

$$|\Psi(t)\rangle = \sum_{m,n} c_{mn} |m, n\rangle, \quad (2.28)$$

where $|m, n\rangle$ is a Fock state of the system with m photons and n phonons. Substituting into Schrödinger equation, the equations for the coefficients c_{mn} are:

$$\begin{aligned} i\dot{c}_{mn}(t) = & (\Delta m + \omega_m n) c_{mn} - gm\sqrt{n}c_{m,n-1} - gm\sqrt{n+1}c_{m,n+1} \\ & + \Omega\sqrt{m}c_{m-1,n} + \Omega^*\sqrt{m+1}c_{m+1,n}, \end{aligned} \quad (2.29)$$

which can be solved after a proper truncation of the Hilbert space.

We solve the mean value equations (2.19) according to the linearized theory, and the quantum equations (2.29) separately for the system initially in its ground state. The quantum equations are solved in a Hilbert space with largest photon number 9 and largest phonon number 7, at which the numerical results converge. After then, we plot in Fig. 2.3 the evolutions of cavity photon numbers $\langle a^\dagger a \rangle$ and phonon numbers $\langle b^\dagger b \rangle$ with different values of coupling strength g . Generally, we

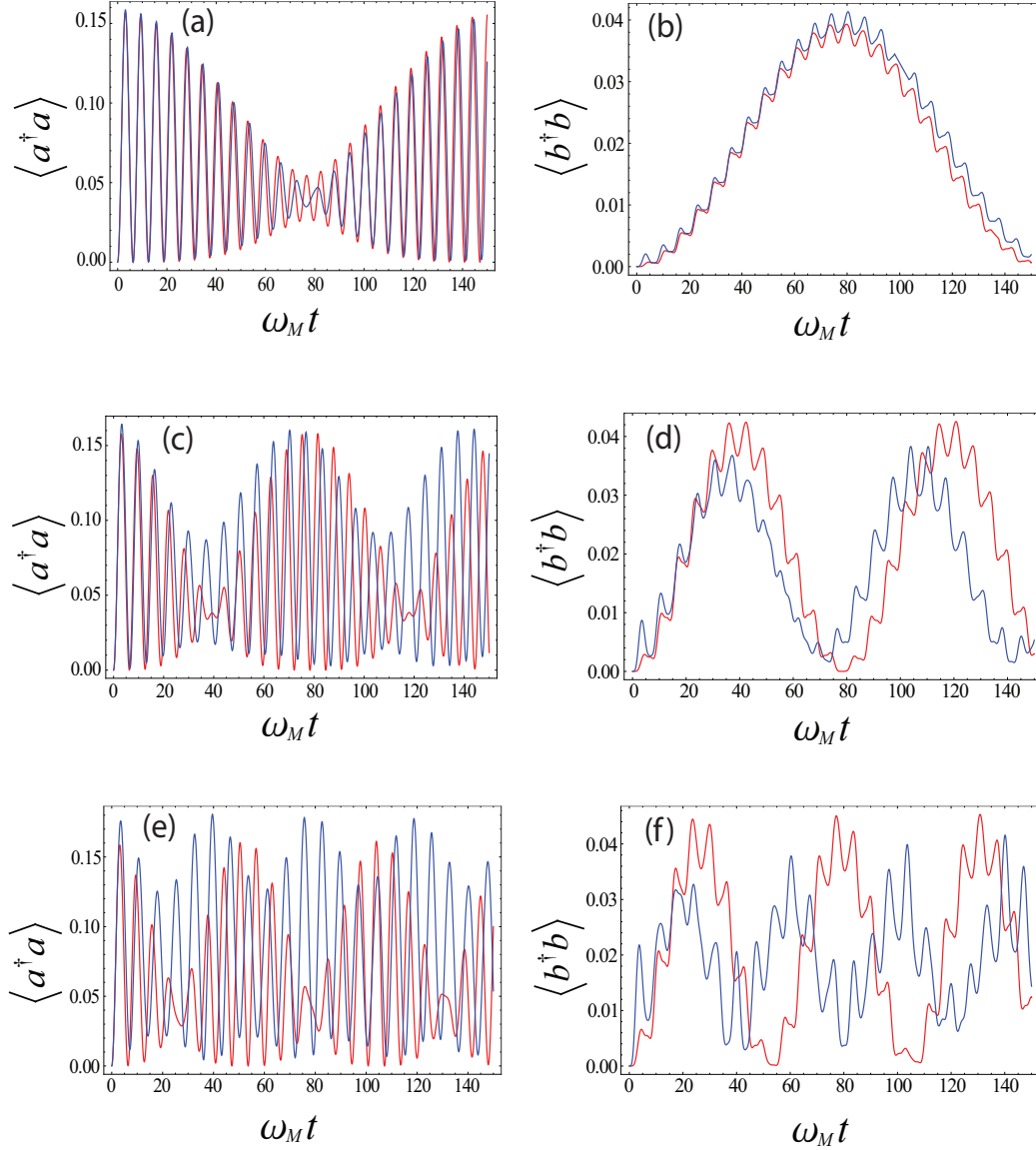


Figure 2.3: Comparison between the linearized theory (red lines) and the exact quantum equations (blue lines) in cavity photon numbers $\langle a^\dagger a \rangle$ and phonon numbers $\langle b^\dagger b \rangle$. Common parameters: $\Delta/\omega_m = 1.01$, $\Omega/\omega_m = 0.2$. Tuned parameter: (a) and (b): $g/\omega_m = 0.1$; (c) and (d): $g/\omega_m = 0.2$; (e) and (f): $g/\omega_m = 0.3$.

see that the cavity photons build up rapidly because of the external driving field, while the phonon numbers gradually grow due to the optomechanical coupling, i.e., the mechanical motion is driven by the radiation pressure of the cavity field. Notably, the fast oscillating patterns in the evolution curves of photon number is mainly caused by the detuning Δ in the linearized equations (2.19), which leads to a fast rotating phase factor. Accordingly, the period of such patterns is about $2\pi/\Delta \approx 2\pi\omega_M^{-1}$ since $\Delta/\omega_M = 1.01$, which agrees well with the Fig. 2.3 (a). In addition, one can see that there are some fast oscillating patterns with small amplitudes in the phonon number evolution curves, which are associated with the fast oscillations of photon number. This is because the phonons are driven by the cavity photons with a rate proportional to photon number, such that the slopes of the phonon number curves also oscillates with the oscillations of photon numbers. Now we compare the results of linearized theory and the exact quantum equations. Note that the differences between the two curves represent the quantum fluctuation accounted by the operator equations (2.20), which is neglected in the linearized theory. First, in Fig. 2.3 (a) and (b), we set the coupling strength as $g = 0.1\omega_M$, which is much smaller than mechanical frequency. We see that the two sets of evolution curves of photon and phonon numbers from the two approaches agree quite well with each other. Next, we tune the coupling strength two times larger: $g = 0.2\omega_M$ in Fig. 2.3 (c) and (d), where we see the difference between the two approaches becomes notable. In Fig. 2.3 (e) and (f), the coupling strength is set to be even larger: $g/\omega_M = 0.3$. In this case, the difference between the two approaches turns out to be so significant that the curves are hardly comparable. For instance, we compare the phonon number at a time $\omega_M t = 80$ in Fig. 2.3 (f), the quantum equation result shows the phonon number is at a minimum, however, the result of linearized theory appears to be a peak value, which is right on the contrary. Hence, we demonstrate that when the coupling strength g become nearly comparable to the mechanical frequency

ω_M , the linearized theory indeed breaks down, or in other words, the linearization condition (2.22) is no longer satisfied. As a result, in the strong coupling regime where coupling strength is comparable to the mechanical frequency ($g \sim \omega_M$), we need to go beyond the linearized theory and take into account the intrinsic non-linearity of the optomechanical coupling so as to explore interesting phenomena of this regime, which is the theme of the studies in this thesis.

2.6 Damping of the System

In this section, we discuss the usual approaches in studying the dissipation of optomechanical systems, including a cavity field damping and a mechanical damping. First, we introduce the Born-Markov master equation, with discussions on approximations made in its derivation and the requirements on physical systems. Then, we provide the specific form of the master equation for our optomechanical systems, which will be used in the studies in this thesis. In addition, we briefly discuss another approach, namely quantum Langevin equation.

The Born-Markov master equation is an approximate equation that describes the dissipative evolution of quantum open systems. The dissipation of a quantum open system is caused by its coupling to the environment, which contains a large number of degrees of freedom. Since an exact calculation of the evolution of the whole system consisting of the concerned system and its environment is neither necessary nor practically accessible, the Born-Markov master equation exploits a strategy to focus on the concerned system only and take into account the effects of the environment without involving its degrees of freedom. To do so, the Born-Markov master equation makes use of two basic assumptions: Born approximation that takes the environment as in a steady state, and Markov approximation that assumes the two-time correlation functions of noise operators to be Dirac delta functions. Such assumptions lead to some requirements on the properties of

the physical system. First, the environment should be large so that it contains a wide spectrum and the environmental state is not affected when coupled to a much smaller system. Additionally, the coupling of the system to its environment should be weak, so that the system density matrix is approximately unchanged within the correlation time.

Now we turn to the damping of optomechanical systems. For the cavity field, damping is caused by the coupling to the outside field, or in other words, the finite cavity mirror transparency. We define the cavity damping rate κ , which means the cavity photons have a lifetime $1/\kappa$. Another source of damping is the mechanical damping of the mirror motion, which originates from various aspects such as viscous damping due to coupling to surrounding gas atoms and excitations of elastic waves in its environments [6]. The dissipation of the mechanical oscillator (mirror) is characterized by a mechanical damping rate γ_M , i.e., the mechanical excitations (phonons) have a lifetime of $1/\gamma_M$. Hence, we model the damping of optomechanical system as two harmonic oscillators coupled to two thermal baths, with the total Hamiltonian given by

$$H_W = H_S + H_B + H_{SB}, \quad (2.30)$$

where H_S and H_B are respectively the Hamiltonian of the optomechanical system and the baths, while H_{SB} describes the coupling between the system and baths. To focus on the evolution of the optomechanical system, we trace out the baths to obtain the reduced density matrix of the system:

$$\rho(t) = \text{Tr}_B [\rho_W(t)], \quad (2.31)$$

where ρ_W is the density matrix of the whole system including the system and baths. We model the baths as consisting of a large number of harmonic oscillators and the system-bath couplings are linear [66]. Under the assumptions that both the cavity field damping and mechanical damping are Markovian processes [50, 35, 67, 68, 70], the evolution of the optomechanical system is described by a

Born-Markov master equation, which is specifically:

$$\begin{aligned} \frac{d\rho}{dt} = & -i[H_S, \rho] - \frac{\kappa}{2} (a^\dagger a \rho - 2a \rho a^\dagger + \rho a^\dagger a) - \frac{\gamma_M(\bar{n}_M + 1)}{2} (b^\dagger b \rho - 2b \rho b^\dagger + \rho b^\dagger b) \\ & - \frac{\gamma_M \bar{n}_M}{2} (b b^\dagger \rho - 2b^\dagger \rho b + \rho b b^\dagger), \end{aligned} \quad (2.32)$$

where \bar{n}_M is thermal phonon number of the bath, and we have assumed thermal photon number $\bar{n}_C = 0$.

For completeness, we mention another widely used approach in studying the dissipative evolution of an optomechanical system: quantum Langevin equation [50, 68, 70]. In contrast to the master equation approach that works in the Schrödinger picture, the Langevin equations are equations of motion of operators in Heisenberg picture [66, 69]. Specifically, for a driven optomechanical system with Hamiltonian given by Eq. (2.16), the quantum Langevin equations describing the dissipative evolution of the annihilation operators of the cavity field mode a and mechanical mode b are [70]:

$$\begin{cases} \dot{a} = -i\Delta a + i g a (b + b^\dagger) - i\Omega - \frac{\kappa}{2} a + a_{in}, \\ \dot{b} = -i\omega_M b + i g a^\dagger a - \frac{\gamma_M}{2} b + b_{in}, \end{cases} \quad (2.33)$$

where a_{in} and b_{in} are respectively the input random noise operator of the cavity field and mechanical modes, with zero expectation values. For a Markovian bath, the noise operators are δ -correlated, with correlation functions given by:

$$\begin{aligned} \langle a_{in}(t) a_{in}^\dagger(t') \rangle &= \kappa \delta(t - t'), \\ \langle a_{in}^\dagger(t) a_{in}(t') \rangle &= 0, \\ \langle b_{in}(t) b_{in}^\dagger(t') \rangle &= \gamma_M (\bar{n}_{thm} + 1) \delta(t - t'), \\ \langle b_{in}^\dagger(t) b_{in}(t') \rangle &= \gamma_M \bar{n}_{thm} \delta(t - t'). \end{aligned} \quad (2.34)$$

Note that we have also assumed the thermal photon number of the bath is zero.

Chapter 3

Single-photon Generation in a Cavity via an Optomechanical Resonance

3.1 Introduction

To manipulate quantum transitions is essential in quantum information processing, which is a prospective application of cavity optomechanics. For such a purpose, researchers have proposed to use optomechanical systems as single-photon sources and single-phonon single-photon transistors [71]. In this chapter, we investigate how one can manipulate quantum transitions between zero- and one-photon states via an optomechanical resonance. An optomechanical resonance is established by a driving laser with its frequency matching the energy difference between a couple of eigenstates of the optomechanical system. We will set up a two-level model and then numerically demonstrate Rabi oscillations between two states of the system. With these Rabi oscillations, we can manipulate the quantum transition from a zero- to one-photon state, such that the optomechanical system can serve as a single-photon source.

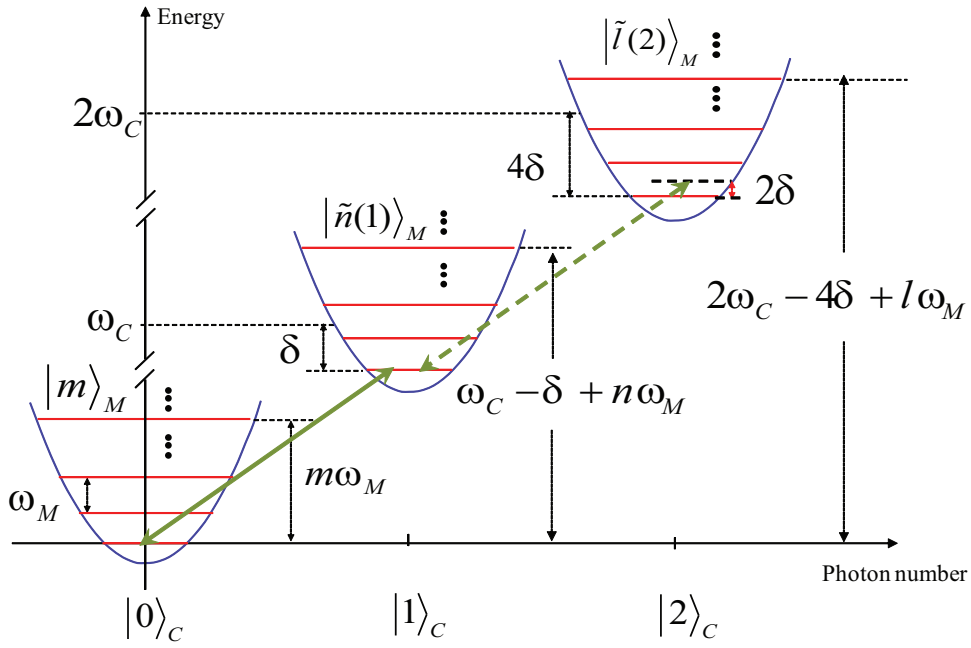


Figure 3.1: Energy-level diagram of an optomechanical system with a laser driving (green arrows) for illustrating photon blockade effect. Here the parameter $\delta = g^2/\omega_M$.

3.2 Two-level Model

In this section, we build up a two-level model of the driven optomechanical system based on the rotating wave approximation (RWA), which operates under the conditions of near-resonance and weak-driving in the single-photon strong coupling regime. Under RWA, we neglect the off-resonant transitions, i.e., the system is confined in a Hilbert space accessed by resonant transitions only.

We consider an optomechanical system driven by an external field with a frequency ω_L and an amplitude Ω . The Hamiltonian of such a driven optomechanical system is given by Eq. (2.15). In a frame rotating at the laser frequency, the Hamiltonian becomes

$$H' = \Delta a^\dagger a + \omega_M b^\dagger b - g a^\dagger a (b^\dagger + b) + \Omega a^\dagger + \Omega^* a, \quad (3.1)$$

where $\Delta = \omega_C - \omega_L$ is the laser detuning, a and b are the annihilation operators of the electromagnetic and mechanical modes, with respective resonant frequency ω_C and ω_M . The first three terms of H' in Eq. (3.1) represent the Hamiltonian of the optomechanical system without the external driving, which can be diagonalized with eigenvectors $|\psi_{n,p}\rangle$ [defined by Eq. (2.13)]. In such eigen basis, the Hamiltonian for the driven optomechanical system can be expressed as

$$H' = \sum_{n,p} \epsilon_{n,p} |\psi_{n,p}\rangle \langle \psi_{n,p}| + \Omega \left(\sum_{n,p,p'} A_{p,p'}^{(n)} |\psi_{n-1,p'}\rangle \langle \psi_{n,p}| + h.c. \right), \quad (3.2)$$

where Ω is assumed to be real for convenience and $\epsilon_{n,p} = n\Delta - n^2 \frac{g^2}{\omega_M} + p\omega_M$. In addition, we have expressed the annihilation operator a in the eigen basis as

$$a = \sum_{n,p} \sum_{n',p'} |\psi_{n,p}\rangle \langle \psi_{n,p}| a |\psi_{n',p'}\rangle \langle \psi_{n',p'}| = \sum_{n,p,p'} A_{p,p'}^{(n)} |\psi_{n-1,p}\rangle \langle \psi_{n,p'}|, \quad (3.3)$$

with the coefficients defined as $A_{p,p'}^{(n)} = \sqrt{n} \langle p| D^\dagger (g(n-1)/\omega_m) D (gn/\omega_M) |p'\rangle$. Explicitly, the coefficients are given by [72]

$$A_{p,p'}^{(n)} = \begin{cases} \sqrt{n} \sqrt{\frac{p!}{p'}} e^{-\frac{\xi^2}{2}} (-\xi)^{p'-p} L_p^{p'-p}(\xi^2), & p \leq p', \\ \sqrt{n} \sqrt{\frac{p!}{p'}} e^{-\frac{\xi^2}{2}} (\xi)^{p-p'} L_{p'}^{p-p'}(\xi^2), & p > p', \end{cases} \quad (3.4)$$

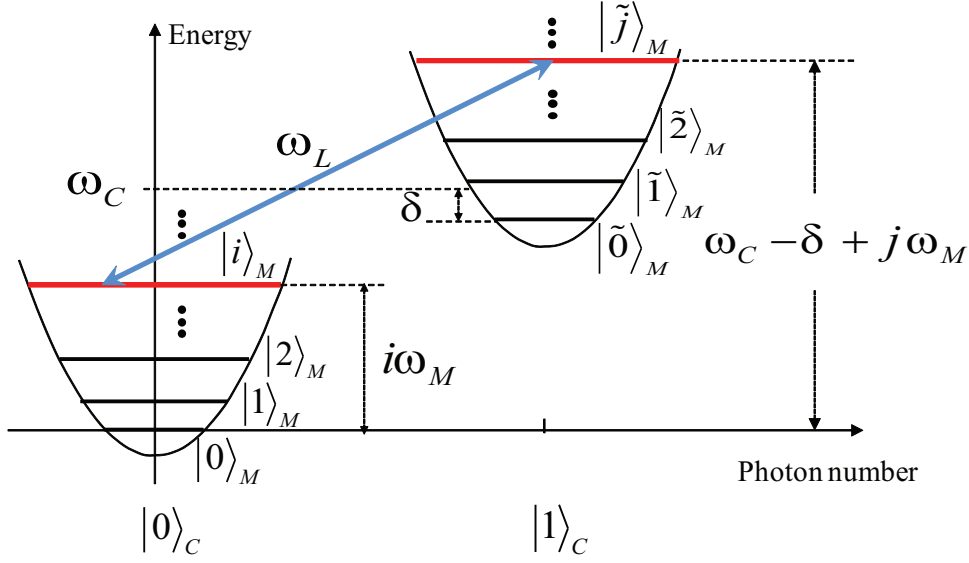


Figure 3.2: Schematic diagram of the two-level model of a driven optomechanical system ($\delta = g^2/\omega_M$).

where $\xi = g/\omega_M$ and $L_r^s(x)$ are associated Laguerre polynomials. Note that for $n = 1$, the coefficient $A_{p,p'}^{(1)}$ is also known as a Franck-Condon factor that represents the overlap between a Fock state and a displaced Fock state. In the literature of molecular physics, a Franck-Condon factor determines the probability of electronic transitions between two states in a vibrational molecule.

Our task is to achieve a two-level model of the driven optomechanical system that only involves the two states: an initial zero-photon state $|\psi_{0,i}\rangle$ and a single-photon state $|\psi_{1,j}\rangle$, with i and j being integers. For such a purpose, the transition between the two states should be set in resonance, while the transitions to states out of the two states are off-resonance. Thus, under rotating wave approximation, we can ignore the off-resonance transitions and take the driven optomechanical system as a two-level system approximately. In order to achieve the resonance, the laser driving frequency should be set to match the energy difference between the two states. This is illustrated in Fig. 3.2, which is drawn in the original frame for simplicity. Hence, we get the resonance condition: $\omega_L = \omega_C - \delta + (j - i)\omega_M$.

Equivalently, the specific laser detuning $\Delta_0 = \omega_C - \omega_L$ satisfying this resonance condition is:

$$\Delta_0 = (i - j)\omega_M + \frac{g^2}{\omega_M}. \quad (3.5)$$

Now that the two states $|\psi_{0,i}\rangle$ and $|\psi_{1,j}\rangle$ are set in resonance, we have to show that the transitions from these two states to other states are off-resonance. The transition from $|\psi_{0,i}\rangle$ to another single-photon state $|\psi_{1,p}\rangle$ ($p \neq j$) has a detuning $|(p - j)\omega_M|$. Similarly, the transition from $|\psi_{1,j}\rangle$ to another zero-photon state $|\psi_{0,q}\rangle$ ($q \neq i$) is detuned by $|(r - i)\omega_M|$. Additionally, we consider the detunings of further excitation from the single-photon state $|\psi_{1,j}\rangle$ to a two-photon state $|\psi_{2,r}\rangle$. Since the energies of the states depend nonlinearly on photon number: $\epsilon_{n,p} = n\Delta - n^2 \frac{g^2}{\omega_M} + p\omega_M$ (as shown in Fig. 3.1), we obtain the detuning of such higher excitation after minor algebra: $|2 \frac{g^2}{\omega_M} + (r - 2j + i)\omega_M|$, which is non-zero generally.

Hence, we see that the dynamics of the system involves two parts: a resonant transition between two states and off-resonant transitions. Accordingly, the Hamiltonian of the system [Eq. (3.1)] can be decomposed into two separate parts:

$$H' = \tilde{H}' + V, \quad (3.6)$$

where \tilde{H}' is resonant part that involves only the two resonant states:

$$\tilde{H}' = \epsilon_{0,i} |\psi_{0,i}\rangle \langle \psi_{0,i}| + \epsilon_{1,j} |\psi_{1,j}\rangle \langle \psi_{1,j}| + \Omega A_{i,j}^{(1)} (|\psi_{0,i}\rangle \langle \psi_{1,j}| + |\psi_{1,j}\rangle \langle \psi_{0,i}|), \quad (3.7)$$

and V accounts for the rest off-resonant part of the Hamiltonian, i.e., $V = H' - \tilde{H}'$. In the weak driving limit, the off-resonant transitions can be neglected according to rotating wave approximation. Specifically, to prevent off-resonant excitations from $|\psi_{0,i}\rangle$ to $|\psi_{1,p}\rangle$ ($p \neq j$), the driving strength should be much smaller than the detuning between the two states: $|(p - j)\omega_M|$, i.e., $\Omega \ll |(p - j)\omega_M|$. In addition, to avoid excitations to 2-photon states $|\psi_{2,q}\rangle$, the weak driving condition is explicitly:

$$\Omega \ll |2g^2/\omega_M - K\omega_M|, \quad (3.8)$$

where K is the nearest integer to $2(g/\omega_M)^2$. For example, if $g < \omega_M/2$ then $K = 0$. Note that since $|2g^2/\omega_M - K\omega_M|$ is always smaller than ω_M , therefore Eq. (3.8) fully describes the weak driving condition. However, we remark that there are some special values of g that leads to the resonance of higher excitations to two-photon states [75]. For a positive integer K , the detuning $|2g^2/\omega_M - K\omega_M|$ can be zero at $g_K = \sqrt{K/2}\omega_M$, such that the excitations of two-photon states become significant. Hence, rigorously speaking, the Eq. (3.8) represents the weak driving condition except for these special values of coupling strength.

In reality, the finite lifetime of the cavity photon should be taken into account. This is because in presence of cavity field damping, the frequency of the cavity photon has a line width, which is equal to the cavity field decay rate κ . In order to have a sharp resonance between the two states, the mechanical sidebands should be resolvable, i.e., $\kappa \ll \omega_M$ (resolved sideband limit). Besides, to prevent higher excitations to two-photon states, the detuning $2g^2/\omega_M$ should also be resolved, i.e., $\kappa \ll 2g^2/\omega_M$. Hence, we require a strong single-photon coupling strength satisfying:

$$g^2 \gg \kappa \cdot \omega_M, \quad (3.9)$$

which characterizes the single-photon strong coupling regime that is needed to avoid the off-resonant transitions.

To summarize, with the driving laser satisfying the resonance condition [Eq. (3.5)] and weak-driving condition [Eq. (3.8)] and a strong optomechanical coupling [Eq. 3.9], the optomechanical system can be modeled by a two-level system consisting of the two resonant states $|\psi_{0,i}\rangle$ and $|\psi_{1,j}\rangle$, neglecting all the off-resonant transitions to other states. Consequently, the Hamiltonian of the system is represented by the resonant part: $H' \approx \tilde{H}'$, i.e., we have

$$H' \approx \epsilon_{0,i} |\psi_{0,i}\rangle \langle \psi_{0,i}| + \epsilon_{1,j} |\psi_{1,j}\rangle \langle \psi_{1,j}| + \Omega_R (|\psi_{0,i}\rangle \langle \psi_{1,j}| + |\psi_{1,j}\rangle \langle \psi_{0,i}|), \quad (3.10)$$

where we define $\Omega_R = \Omega A_{i,j}^{(1)}$ (note that $\epsilon_{0,i} = \epsilon_{1,j}$). Thus, we obtain the two-level

model of the driven optomechanical system.

3.3 Rabi Oscillations in an Ideal Cavity

In this section, we investigate a direct implication of the two-level Hamiltonian: Rabi oscillations between two states. In order to clearly study the efficiency of the two-level model, we first focus on the coherent evolution of the system in an ideal cavity without damping.

As an representative example, we study a specific Rabi oscillation between the two states: the ground state $|\psi_{00}\rangle$ and an excited state $|\psi_{11}\rangle$. For this case, the resonant condition [Eq. (3.5)] is specifically: $\Delta_0 = \frac{g^2}{\omega_M} - \omega_M$. Together with the weak driving condition Eq. (3.8), we achieve the two-level Hamiltonian H' given by Eq. (3.10) with $i = 0$ and $j = 1$. Thus, the time evolution of the system is governed by the Schrödinger equation (with $\hbar = 1$): $i|\dot{\Psi}(t)\rangle = H'|\Psi(t)\rangle$, with H' the two-level Hamiltonian. Let the initial state of the system be: $|\Psi(0)\rangle = |\psi_{0,0}\rangle$, then the system state at time t is given by

$$|\Psi(t)\rangle = \cos \Omega_R t |\psi_{00}\rangle - i \sin \Omega_R t |\psi_{11}\rangle, \quad (3.11)$$

which exhibits Rabi oscillations with the Rabi frequency $\Omega_R = \Omega A_{0,1}^{(1)} = -\Omega \xi e^{-\frac{\xi^2}{2}}$ according to Eq. (3.4), and we have $\epsilon_{0,0} = \epsilon_{1,1} = 0$. In addition, the system evolves into the single-photon state ψ_{11} at the time T_0 :

$$T_0 = \frac{\pi}{2\Omega_R} = \frac{\pi}{2\Omega\xi} e^{\frac{\xi^2}{2}}, \quad (3.12)$$

which is inversely proportional to the driving strength Ω and the Franck-Condon factor $A_{0,1}^{(1)}$. Hence, such Rabi oscillations can be used to generate a single cavity photon starting from vacuum.

3.4 Numerical Results

In this section, we perform numerical calculations to verify the validity of the two-level model and quantitatively study the efficiency of single-photon generation.

Since the optomechanical system actually consists of a large number of eigenstates, there can be many possible transitions in reality. In order to verify the approximate Hamiltonian and to show that the off-resonant transitions can indeed be neglected, we perform numerical simulations of the coherent dynamics based on the original Hamiltonian in an ideal cavity without cavity field and mechanical dampings. The observation of Rabi oscillations in the evolution of the system is regarded as the signature of the two-level Hamiltonian. In addition, we compare the oscillation periods between the numerical simulation results and model prediction as a quantitative evidence of the efficiency of the model. After then, we investigate the dependence of the single-photon generation on the driving strength and its sensitivity to small variations of laser detuning.

We solve numerically the Schrödinger equation $i|\dot{\Psi}(t)\rangle = H'|\Psi(t)\rangle$ with H' the original Hamiltonian given by Eq. (3.1). Expanded in a certain basis, the Schrödinger equation is equivalent to a set of coupled differential equations of the probability amplitudes, which can be solved numerically with MATHEMATICA after an appropriate truncation of the Hilbert space. In the simulations discussed below, we use a Hilbert space in which the largest photon number is set as 3 and the largest phonon number is 8, which we find the results converge.

In order to demonstrate the Rabi oscillations between the two states, we plot in Fig. 3.3 time evolutions of probability P of being in the single-photon state $|\psi_{11}\rangle$:

$$P = |\langle\psi_{1,1}|\Psi(t)\rangle|^2. \quad (3.13)$$

Particularly, for a system whose time evolution is given by Eq. (3.11), the single-photon probability is $P(t) = \sin^2 \Omega_R t$, i.e., a sinusoidal function of time.

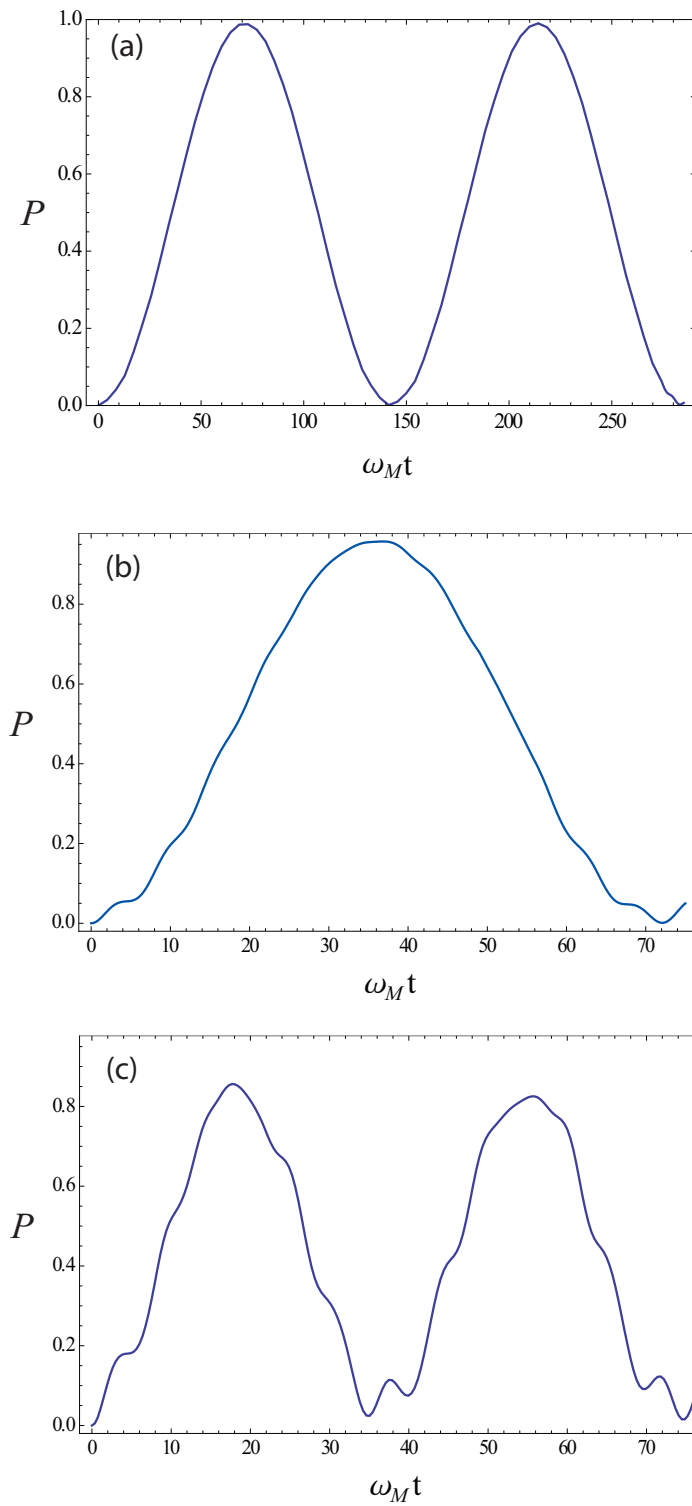


Figure 3.3: Time evolution of single-photon probability. Parameters are set as: $g/\omega_M = 0.5$, $\Delta_0/\omega_M = -0.75$; (a) $\Omega/\omega_M = 0.05$; (b) $\Omega/\omega_M = 0.1$; (c) $\Omega/\omega_M = 0.2$.

Fig. 3.3 (a) shows a typical Rabi oscillation that the probability P of being in single-photon state oscillates sinusoidally and the maximum value reaches near 1. Hence, our two-level model fits well for this case where $\Omega/\omega_M = 0.05$. In Fig. 3.3 (b) and (c), we plot the single-photon probability P curves with two larger driving strengths. One can see that some small oscillation patterns appear in the roughly sinusoidal curves. Such patterns are caused by off-resonant transitions, which become more significant with larger driving strengths. Moreover, the maximal values of single-photon probability decline significantly, especially for the case with $\Omega/\omega_M = 0.2$, whose maximal probability is about 0.85. Note that the weak driving condition Eq. (3.8) requires: $\Omega \ll 0.5\omega_M$. The numerical results demonstrate that such a requirement is indeed necessary and the two-level model is indeed effective when such weak driving condition is satisfied.

To further confirm the validity of the two-level model, we compare in Fig. 3.4 the dependence of T_0 on driving amplitude Ω and coupling strength g between numerical results and model predictions. The curves are drawn according to the prediction of the two-level model given in Eq. (3.12). It is shown that T_0 declines both with larger Ω and g (for $0 < g/\omega_M < 1$) and the analytical and numerical results agree well with each other. Notice that the small deviations between the numerical and analytical results are caused by off-resonance transitions. Such consistence provides an additional evidence for the validity of the two-level model.

Finally, we investigate the performance of the single-photon generation with small deviations of the laser detuning Δ from Δ_0 . For such a purpose, we plot in Fig. 3.5 the maximal single-photon probabilities P_{max} during a Rabi oscillation versus off-resonance value of the laser detuning: $\tilde{\Delta} = \Delta - \Delta_0$. It is shown that the maximal single-photon probabilities P_{max} peaked at the resonance detuning ($\tilde{\Delta} \approx 0$), and declines when the $|\tilde{\Delta}|$ becomes larger. Notice that the peak does not locate exactly at $\tilde{\Delta} = 0$, because the energy difference in the two-level model is slightly shifted due to off-resonant couplings with other states. As a theoretical

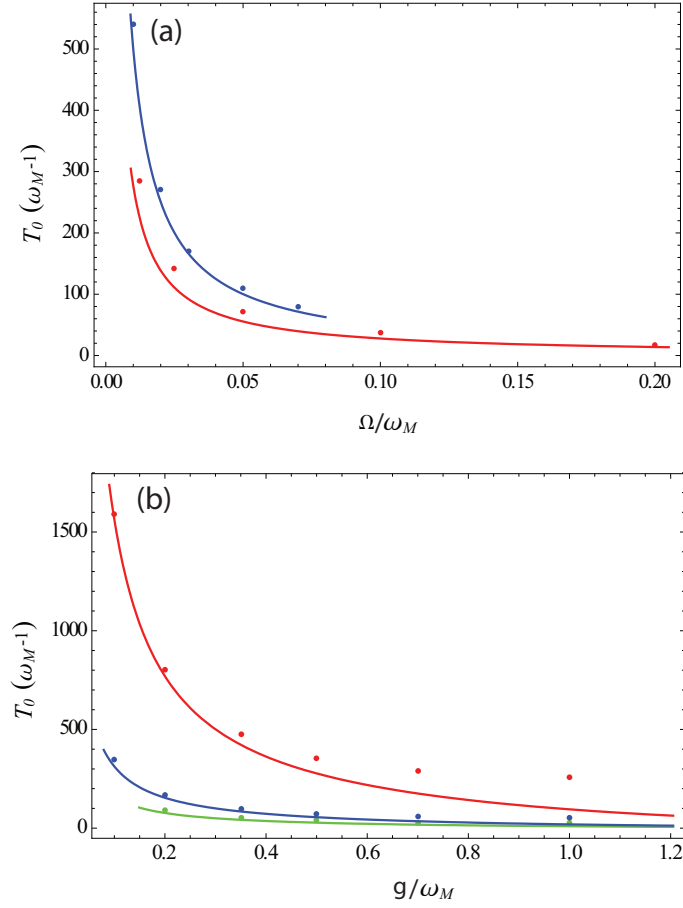


Figure 3.4: Compare of T_0 between analytical result of the model (lines) and numerical calculations (dots). Parameters are set as: (a) Red line: $g/\omega_M = 0.5$, Blue line: $g/\omega_M = 0.3$; (b) Green line: $\Omega/\omega_M = 0.1$, blue line: $\Omega/\omega_M = 0.05$, red line: $\Omega/\omega_M = 0.01$.

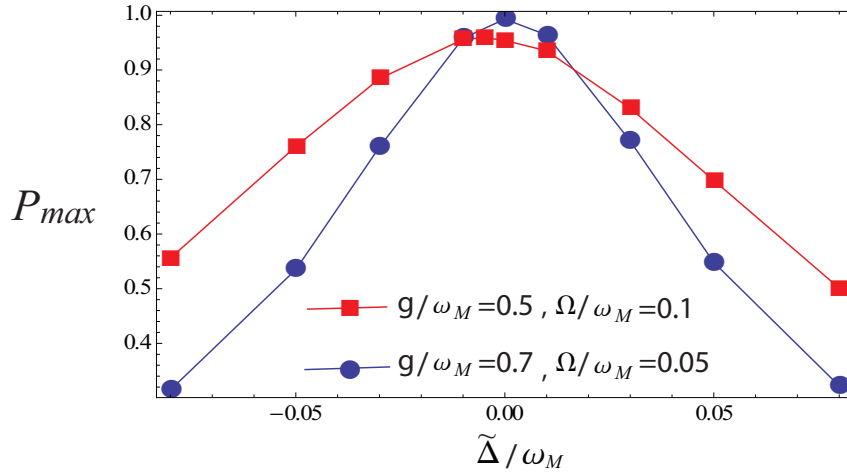


Figure 3.5: Maximal probability of the single-photon state P_{max} as a function of off-resonance detuning $\tilde{\Delta}$. Parameters are set as: square: $g/\omega_M = 0.5$, $\Omega/\omega_M = 0.1$; circle: $g/\omega_M = 0.7$, $\Omega/\omega_M = 0.05$.

expectation, if the two-level model is exact, i.e., there are no off-resonance effects, then the maximal probability should be $P_{max} = \Omega_R^2 / (\Omega_R^2 + \tilde{\Delta}^2)$, which means the performance is determined by the ratio between the detuning and driving amplitude and quantitatively the half value of P_{max} locates at $|\tilde{\Delta}| = \Omega_R$. This is consistent with our numerical results. For example, P_{max} decreases faster in the case $\Omega/\omega_M = 0.05$ (circles) than that in $\Omega/\omega_M = 0.1$ (square). In addition, for the case $\Omega/\omega_M = 0.05$ (circles), P_{max} decreases to about the half value 0.5 at the detuning $\tilde{\Delta} = \Omega$.

3.5 Effects of Cavity Field Damping

In this section, we study the performance of single-photon generation against cavity field damping, which is inevitable in experiments. Here we ignore the mechanical damping, because mechanical damping rate is usually much smaller than cavity field damping. In typical experiments, the lifetime of a mechanical

excitation (phonon) is of the order $10^4\omega_M^{-1}$, which is much longer than the time period of single-photon generation $T_0 \sim 100\omega_M^{-1}$. However, the lifetime of a cavity photon can be comparable to the time period T_0 . Hence, we focus on the effects of cavity field damping on a single-photon generation process.

The dissipative evolution of the optomechanical system with cavity field damping governed by the master equation:

$$\frac{d\rho}{dt} = -i[H', \rho] - \frac{\kappa}{2} (a^\dagger a \rho - 2a\rho a^\dagger + \rho a^\dagger a), \quad (3.14)$$

where ρ is the density matrix of system defined as $\rho = \sum_{m,n} \sum_{m',n'} \rho_{m,n,m',n'} |m,n\rangle \langle m',n'|$, with $|m,n\rangle$ being a Fock state with m photons and n phonons. κ is the decay rate of the cavity field, and H' is the Hamiltonian describing the driven optomechanical system given by Eq. (3.1). In order to do numerical calculations, we substitute the ρ into the master equation (3.14) and then obtain the equations of motion for the elements $\rho_{m,n,m',n'}$. To show explicitly the cavity photon decay process, here we set the driving field as a pulse, which is turned off at the time T_0 when the maximal single-photon probability P is reached. Here we use the same size of Hilbert space as the simulations done in the previous section: the largest photon number is set as 3 and the largest phonon number is 8.

To study the influences of cavity field damping to the performance of single-photon generation, we set the optomechanical system be driven by a pulse with the driving amplitude defined as a step function: $\Omega(t) = \Omega_0 \cdot \theta(T_0 - t)$. Such a setting means that when $t < T_0$, the system is constantly driven by a laser with an amplitude Ω_0 ; however, the laser driving is turned off at $t = T_0$ when the maximal probability of the single-photon state is reached. In Fig. 3.6, we plot the evolutions of the single-photon state probability P for different decay rates, together with a zero-damping case (black line) for reference. It is shown that in the constant driving period ($t < T_0$), the fidelities keep growing and reach the maximal values at $t = T_0$. After the laser driving is turned off ($t > T_0$), the single-photon state fidelities decay due to the cavity field damping, i.e., the

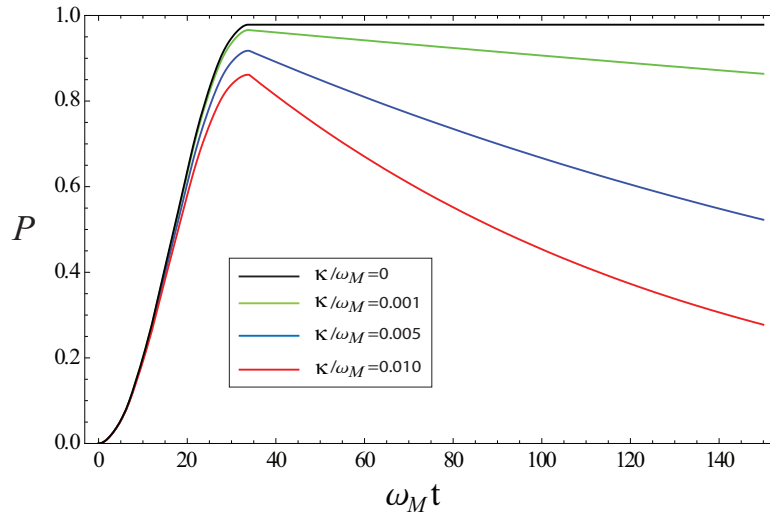


Figure 3.6: Evolution of the single-photon state probability P for different decay rates in a pulse-driving optomechanical system. Parameters are set as: $g/\omega_M = 0.55$, $\Omega/\omega_M = 0.055 \cdot \theta(T_0 - t)$, where $\theta(T_0 - t)$ is a step function and $T_0 = 34\omega_M^{-1}$.

cavity photon gradually leaks out of the cavity. Notably, the maximal value of the fidelities for the case without cavity field damping (black curve) is the largest, reaching about 0.98. However, when the cavity field damping rate becomes larger, the maximal probability decreases significantly. In particular, the maximal probability decreases to about 0.85 for $\kappa/\omega_M = 0.010$. But for a smaller decay rate $\kappa/\omega_M = 0.001$, the maximal probability still reaches more than 0.95, i.e., the single-photon state is reached largely. Hence, the effects of cavity field damping to single-photon generations can be negligibly small when the field decay rate is sufficiently small. Specifically, the decay rate should satisfy: $1/\kappa \gg T_0$, meaning that the lifetime of the cavity photons should be much larger the time period T_0 .

3.6 Connection to Photon Blockade Effect

The mechanism of the two-level model is closely related to the photon blockade effect, which has been identified by P. Rabl [48]. For this reason, we describe

Rabl's work and then make a connection of our study to this effect. Rabl identified photon blockade effect as a fundamental mechanism in the single-photon strong coupling regime of cavity optomechanics. It is claimed that for a weakly driven optomechanical system in the combined regime of single-photon strong coupling and resolved sidebands, the existence of a single cavity photon resists the excitation of a second photon inside the cavity.

Rabl provided an intuitive picture of the photon blockade effect by analyzing the photon excitations based on the energy level diagram. The arguments are similar to our discussion in section 2. Basically, when a single-photon excitation is set in resonance, then the excitation of a second photon off-resonant by $2g^2/\omega_M$. Thus, two-photon excitations can be suppressed under the condition $g^2/\omega_M > \kappa$ in the weak driving limit, leading to the photon blockade effect. Such a mechanism is essentially the same with our two-level model, together with similar conditions shown in Eq. (3.5), Eq. (3.8) and Eq. (3.9).

In addition, to justify such photon blockade effect, Rabl performed analytic calculations of two-photon equal time correlation function $g^{(2)}(0)$ upon some leading term approximations. The physical meaning of the $g^{(2)}(0)$ function is the ratio between two-photon joint detection probability and the product of single-photon detection probability. For a single-mode cavity field at the same space-time point, the $g^{(2)}(0)$ function is defined as

$$g^{(2)}(0) = \frac{\langle a^\dagger a^\dagger a a \rangle}{\langle a^\dagger a \rangle^2} = \frac{\text{Tr}(\rho a^\dagger a^\dagger a a)}{[\text{Tr}(\rho a^\dagger a)]^2}, \quad (3.15)$$

which is an indicator of antibunching effect when $g^{(2)}(0) < 1$, and $g^{(2)}(0) \rightarrow 0$ means a full photon blockade. According to the calculation result, the correlation function $g^{(2)}(0)$ indeed has values smaller than 1, i.e., photon antibunching effects are observed. In addition, it is found that to achieve the photon antibunching $g^{(2)}(0) < 1$, the conditions of strong coupling $g > \kappa$ and resolved sidebands $\kappa < \omega_M$ are necessary.

We evaluate the two-photon equal time correlation function $g^{(2)}(0)$ in our Rabi

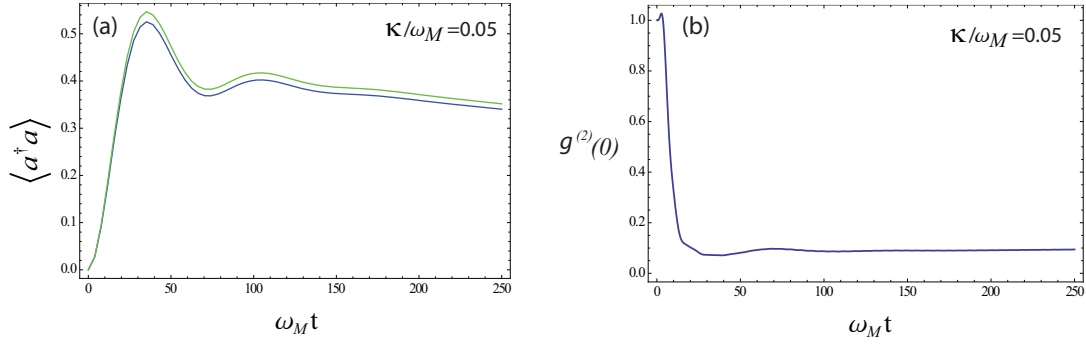


Figure 3.7: Evolutions of (a) average photon numbers and (b) two-photon equal time correlation function $g^{(2)}(0)$. The green line in (a) is the total number of photons in the cavity, while the blue one is the number only takes into account photons in single-photon states. Parameters are set as: $g/\omega_M = 0.50$, $\Omega/\omega_M = 0.05$, $\Delta/\omega_M = 0.25$, $\kappa/\omega_M = 0.05$.

oscillations. Based on the master equation simulation, we plot in Fig. 3.7 the cavity photon numbers and correlation function $g^{(2)}(0)$ as functions of time. The initial state of the system is set to be the ground state, i.e., $|\Psi(0)\rangle = |\psi_{00}\rangle$ and the parameters are so set to achieve the Rabi oscillation between $|\psi_{00}\rangle$ and $|\psi_{10}\rangle$. In Fig. 3.7 (a), the green curve represents the evolution of total cavity photon number, while the blue curve is the evolution of photon number which only takes into account photons in single-photon states but excludes multi-photon states. We can see that the difference between the two curves are very small, meaning that most photons are in single-photon states and the excitation of multi-photon states are very low. Fig. 3.7 (b) shows the evolution of the correlation function $g^{(2)}(0)$. We see that $g^{(2)}(0)$ decreases quickly from 1 to about 0.1 in a time $t = 20\omega_M^{-1}$ and then maintains such a small value. Thus, we indeed observe significant features of photon blockade effect in the Rabi oscillation process. In addition, the system is set in the strong coupling regime that $g = 0.5\omega_M \gg \kappa = 0.05\omega_M$ and the resolved sideband regime that $\kappa < \omega_M$, which is consistent with the requirements of Rabl's photon blockade theory.

3.7 Conclusion

To conclude, we have built up a two-level model with a resonant condition [Eq. (3.5)] under the weak driving condition [Eq. (3.8)] and a strong optomechanical coupling strength [Eq. 3.9]. With such a model, we are able to generate a single cavity photon from a zero-photon state of the system via Rabi oscillations. We demonstrate these Rabi oscillations with numerical simulations based on the Schrödinger equation. In addition, we investigate the dependence of the Rabi oscillations on driving strength and its sensitivity to small deviation of the laser detuning. Moreover, we study the effects of cavity field damping to the single-photon generation with master equation (3.14) simulations and show that when the decay rate $\kappa \ll 1/T_0$ the effect of cavity field damping is negligible. At last, we make a connection of our study in this chapter to a closely related phenomenon called photon blockade effect. Specifically, we illustrate with numerical examples that the photon blockade effect is observed in the Rabi oscillation process.

Chapter 4

Optomechanical Dark States

4.1 Introduction

Coherent population trapping (CPT) in a dark state [80, 81] is a quantum coherent effect in which a system does not absorb photons from external driving fields because of a destructive interference. A closely related phenomenon is electromagnetically induced transparency (EIT) [82], which shares the same underlying mechanism of quantum interference but with a different realizing scheme. CPT and EIT has been comprehensively studied in atomic systems, which can lead to dramatic modifications of optical properties of a medium. As an analogy in cavity optomechanics, researchers have proposed optomechanically induced transparency that in presence of a strong control laser, the absorption of a weak probe laser by the optomechanical system can be very small [27, 28]. Notably, such an optomechanically induced transparency phenomenon has been observed in experiments recently [30, 29, 31, 32]. In such a process, there are significant excitations of cavity photons and phonons (mechanical excitations) due to the strong control laser, which can be analyzed by the linearized theory (see chapter 2.4).

In this chapter, we investigate dark states of cavity optomechanical systems in the single-photon strong coupling regime [86], where the linearized theory

is not applicable. We study an optomechanical system that is driven by two laser fields. We first achieve an effective Hamiltonian under some resonance conditions, and then we show that with a set of special values of optomechanical coupling strengths we can confine the effective Hamiltonian in a finite Hilbert space. Furthermore, we derive an analytical form of the dark state, which is a special eigenvector of the effective Hamiltonian with zero eigenenergy. Such dark states are stable states of the driven system with zero photon in the cavity. In addition, we illustrate with numerical simulations that these dark states can be prepared by optical pumping, which makes use of the decay of cavity photons. Besides, we also study the influence of mechanical damping to the efficiency of optical pumping into a dark state.

4.2 Review of Dark States in Three-level Systems

In this section, we make a brief review of the background of dark states and coherent population trapping [80] in atomic physics.

Typically, dark states are discussed in a Λ -type three-level atom, with the energy-level structure shown in the Fig. 4.1. The states $|1\rangle$ and $|2\rangle$ are two ground states, the transition between which is dipole-forbidden. The state $|3\rangle$ is an excited state, and the atomic transitions $|1\rangle \rightarrow |3\rangle$ and $|2\rangle \rightarrow |3\rangle$ are dipole-allowed. Such a Λ atom is driven by two laser fields, with comparable driving strengths Ω_p and Ω_q . The frequencies of the lasers ω_p and ω_q are set to be near-resonant with $|1\rangle \rightarrow |3\rangle$ and $|2\rangle \rightarrow |3\rangle$ transition respectively, with a small common detuning Δ . Consequently, a Raman resonance between the state $|1\rangle$ and $|2\rangle$ is achieved. The Hamiltonian of such a driven atom under rotating wave

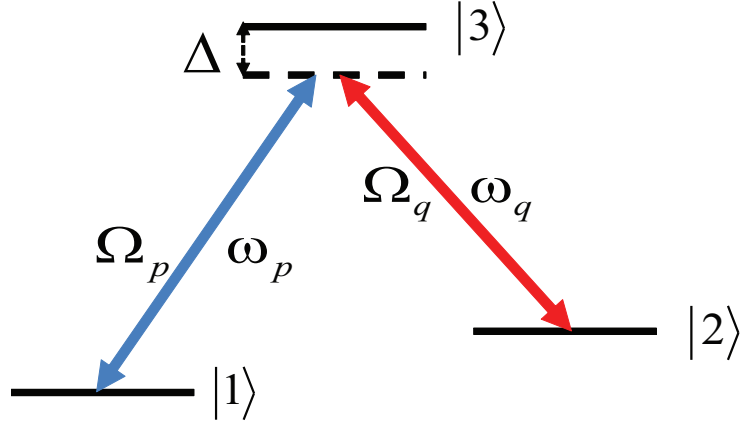


Figure 4.1: Energy-level diagram of a Λ -type three-level atom driven by two near-resonant lasers.

approximation is:

$$H = \omega_1 |1\rangle \langle 1| + \omega_2 |2\rangle \langle 2| + \omega_3 |3\rangle \langle 3| + (\Omega_p e^{-i\omega_p t} |3\rangle \langle 1| + H.c.) + (\Omega_q e^{-i\omega_q t} |3\rangle \langle 2| + H.c.). \quad (4.1)$$

To obtain a time-independent Hamiltonian, we go to a rotating frame defined by the unitary operator $U = \exp\{-i[\omega_1 |1\rangle \langle 1| + \omega_2 |2\rangle \langle 2| + (\omega_p + \omega_1) |3\rangle \langle 3|]t\}$. The transformed Hamiltonian is

$$\tilde{H} = \Delta |3\rangle \langle 3| + (\Omega_p |3\rangle \langle 1| + H.c.) + (\Omega_q |3\rangle \langle 2| + H.c.), \quad (4.2)$$

where we have used the Raman resonance condition: $\Delta = \omega_3 - \omega_1 - \omega_p = \omega_3 - \omega_2 - \omega_q$. The Hamiltonian \tilde{H} has a special eigenvector $|D\rangle$ with zero eigenvalue, satisfying:

$$\tilde{H} |D\rangle = 0. \quad (4.3)$$

Explicitly, this eigenvector is given by (assuming real Ω_p and Ω_q for convenience):

$$|D\rangle = \frac{1}{\sqrt{\Omega_p^2 + \Omega_q^2}} (\Omega_q |1\rangle - \Omega_p |2\rangle), \quad (4.4)$$

which only involves the two ground states $|1\rangle$ and $|2\rangle$, while the probability in the excited state $|3\rangle$ is zero. Such an eigenstate of a Λ -type three-level system is

called a dark state in the sense that it is a stable state in which the atom does not absorb or emit photons during its interaction with the driving lasers. Intuitively, such a non-absorption is because the excitations to $|3\rangle$ have contributions from the states $|1\rangle$ and $|2\rangle$ separately with a phase difference, such that the summation of the two contributions cancels exactly. Therefore, the coherence in the atomic state is the basis of the dark states phenomenon. Note that the dark states are closely related to electromagnetically induced transparency (EIT) [84, 85]. If the atom is in the dark state, then it is transparent to external driving fields.

In addition, dark states can be prepared by optical pumping in experiments [81, 83]. An optical pumping scheme makes use of the spontaneous decay of the excited state $|3\rangle$. Since there is always probability that the excited state decays into the dark state and the dark state is stable, then the probability of the system being in the dark state will accumulate to 1, i.e., the system is optically pumped into the dark state gradually.

4.3 The Model

We consider an optomechanical cavity which is driven by two lasers with frequencies ω_1 and ω_2 , as shown in Fig. 4.2. The Hamiltonian of such a driven system is given by

$$H = \omega_c a^\dagger a + \omega_M b^\dagger b - g a^\dagger a (b^\dagger + b) + [(\Omega_1 e^{-i\omega_1 t} + \Omega_2 e^{-i\omega_2 t}) a^\dagger + H.c.], \quad (4.5)$$

where a (b) and ω_c (ω_M) are respectively the annihilation operator and resonant frequency of the cavity field (mechanical) modes, and we have set $\hbar = 1$. The Ω_1 and Ω_2 are proportional to the amplitudes of the external fields. Generally, without specifically chosen laser frequencies, the system will be driven such that both numbers of cavity photons and phonons keep growing. However, we will show that with specially chosen laser frequencies, the system can evolve into a stable dark state. In the frame rotating at the frequency ω_c , the transformed

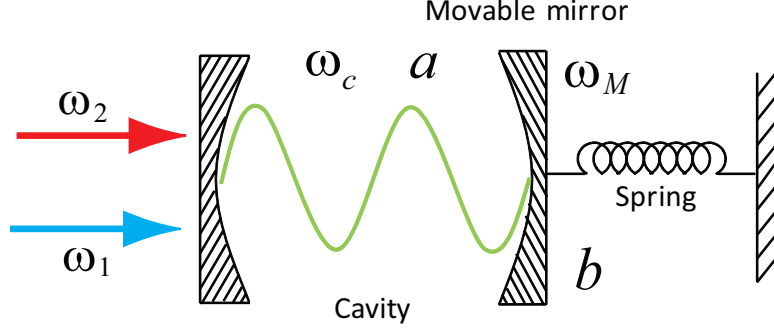


Figure 4.2: Schematic diagram of an optomechanical system consisting of a fixed end mirror and a movable end mirror with two driving fields.

Hamiltonian reads

$$H_r = \omega_M b^\dagger b - g a^\dagger a (b^\dagger + b) + [(\Omega_1 e^{-i\Delta_1 t} + \Omega_2 e^{-i\Delta_2 t}) a^\dagger + H.c.], \quad (4.6)$$

where the detunings $\Delta_1 = \omega_1 - \omega_c$ and $\Delta_2 = \omega_2 - \omega_c$ are defined. The first two terms of H_r correspond to the Hamiltonian H_0 without driving, and it can be diagonalized in the displaced basis as Eq. (2.14), with the eigenvectors of H_0 : $|\psi_{n,p}\rangle$ given in Eq. (2.13). Here the energy eigenvalues of H_0 are $\varepsilon_{n,p} = p\omega_M - n^2 g^2 / \omega_M$, which depend nonlinearly on photon number n , and linearly on phonon number p .

In the eigenbasis of H_0 , the Hamiltonian H_r in Eq. 4.6 is given by

$$H_r = \sum_{n,p} \varepsilon_{n,p} |\psi_{n,p}\rangle \langle \psi_{n,p}| + \sum_{n,p,p'} \left[A_{p,p'}^{(n)} (\Omega_1 e^{-i\Delta_1 t} + \Omega_2 e^{-i\Delta_2 t}) |\psi_{n,p'}\rangle \langle \psi_{n-1,p}| + H.c. \right], \quad (4.7)$$

where we have expressed the annihilation operator a in the eigenbasis as Eq. 3.3 with the coefficients $A_{p,p'}^{(n)} = \sqrt{n} \langle p | D(g/\omega_M) | p' \rangle$. The explicit form of the coefficients is given by Eq. 3.4. For simplicity, we go to the interaction picture

where the Hamiltonian in Eq. 4.7 is transformed to be:

$$\begin{aligned}
H'_r &= e^{iH_0t} H_r e^{-iH_0t} - H_0 \\
&= \sum_{n,p,p'} \left[A_{p,p'}^{(n)} \left(\Omega_1 e^{i(\varepsilon_{n,p'} - \varepsilon_{n-1,p} - \Delta_1)t} + \Omega_2 e^{i(\varepsilon_{n,p'} - \varepsilon_{n-1,p} - \Delta_2)t} \right) |\psi_{n,p'}\rangle \langle \psi_{n-1,p}| \right. \\
&\quad \left. + H.c. \right], \tag{4.8}
\end{aligned}$$

with H_0 the Hamiltonian of the system without driving.

4.4 Effective Hamiltonian in a Confined Hilbert Space

In this section, we derive an effective Hamiltonian that operates in a finite dimensional Hilbert space. This is achieved by making use of resonance transitions and the dependence of transition matrix elements on the coupling strength g .

4.4.1 Resonant Hamiltonian under RWA

Now we show that under conditions of resonance and weak driving, we can achieve a resonant Hamiltonian according to rotating wave approximation (RWA).

First of all, we assume that the cavity field decay rate κ is much smaller than ω_M , i.e., in the resolved sidebands regime that $\kappa \ll \omega_M$. To achieve a set of resonant transitions, we set the laser frequencies ω_1 and ω_2 such that the detunings of the lasers Δ_1 and Δ_2 satisfying the following resonance conditions:

$$\Delta_1 = \varepsilon_{1,p} - \varepsilon_{0,p} = -g^2/\omega_M, \tag{4.9}$$

$$\Delta_2 = \varepsilon_{1,p} - \varepsilon_{0,p+1} = -\omega_M - g^2/\omega_M. \tag{4.10}$$

which means that the laser with frequency ω_1 matches the energy difference between the states $|\psi_{0,p}\rangle$ and $|\psi_{1,p}\rangle$, while the other laser establishes a resonance transition between the states $|\psi_{1,p}\rangle$ and $|\psi_{0,p+1}\rangle$, with $p = 0, 1, 2, \dots$. Such a resonant coupling scheme is illustrated in Fig. 4.3. Hence, we see that the transitions

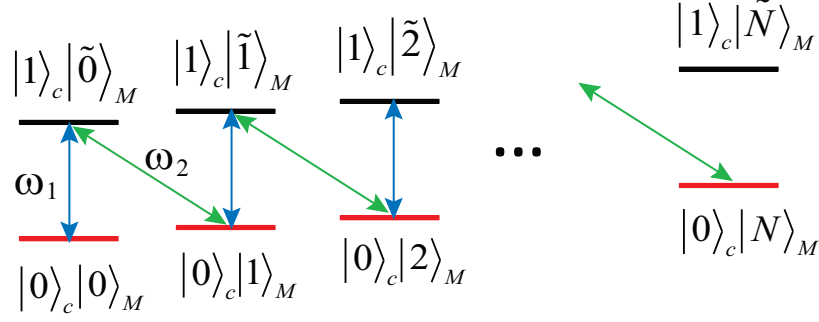


Figure 4.3: The coupling scheme between energy levels of the optomechanical system (only zero- and one-photon states are shown). Here each laser is used to establish a set of resonant transitions, and $|p\rangle_M = |\tilde{p}(0)\rangle_M$ and $|\tilde{p}\rangle_M = |\tilde{p}(1)\rangle_M$ for simplicity. By choosing $g = g_N$, there is no transition between $|0\rangle_c|N\rangle_M$ and $|1\rangle_c|\tilde{N}\rangle_M$.

between the states can be divided into two kinds: one is the resonant transitions and the other is off-resonant transitions. In such a spirit, we can decompose the Hamiltonian of the driven system into two parts as:

$$H'_r = \tilde{H}'_r + V, \quad (4.11)$$

where \tilde{H}'_r is the composition that describes resonant transitions, which is explicitly

$$\tilde{H}'_r = \sum_p \left[(A_{p,p}^{(1)} \Omega_1 |\psi_{1,p}\rangle \langle \psi_{0,p}| + A_{p+1,p}^{(1)} \Omega_2 |\psi_{1,p}\rangle \langle \psi_{0,p+1}|) + H.c. \right], \quad (4.12)$$

while V describes the off-resonance transitions, which can be expressed as

$$V = \sum'_{n,p,p'} \left[A_{p,p'}^{(n)} \left(\Omega_1 e^{i\delta_1(n,p,p')t} + \Omega_2 e^{i\delta_2(n,p,p')t} \right) |\psi_{n,p'}\rangle \langle \psi_{n-1,p}| + H.c. \right]. \quad (4.13)$$

Here the primed summation in V excludes those terms in \tilde{H}'_r , i.e., $V = H'_r - \tilde{H}'_r$.

In particular, we have defined the off-resonance detunings of these transitions as:

$$\delta_1(n, p, p') = (p' - p)\omega_M - \frac{2g^2}{\omega_M}(n - 1), \quad (4.14)$$

$$\delta_2(n, p, p') = (p' - p + 1)\omega_M - \frac{2g^2}{\omega_M}(n - 1). \quad (4.15)$$

If these detunings $\delta_j(n, p, p')$ are sufficiently large compared with the driving strengths Ω_j , then the off-resonant transitions described by V can be neglected according to the rotating wave approximation. In other words, under a weak driving limit that $\Omega_j \ll \delta_j(n, p, p')$, only the resonant transitions described by \tilde{H}'_r are significant. As a result, if the cavity is initially in the ground state, then there will only be those significant transitions shown in Fig. 4.3, i.e., the system is confined to the zero and single photon states. Such a phenomenon shares the same mechanism as the photon blockade effect [48], which relies on the fact that the excitations from 1- to 2-photon states are far off-resonance. In particular, in order to neglect the transitions from 1-photon to 2-photon states, the matrix element coupling the states should be much smaller than the corresponding detuning, i.e., $A_{p,p'}^{(2)}\Omega_j \ll \delta_j(2, p, p')$. Since the coefficient $A_{p,p'}^{(2)} \sim 1$, then the weak driving condition is merely

$$\Omega_j \ll \min(|2g^2/\omega_M - K\omega_M|) \quad (4.16)$$

for $j = 1, 2$, and the minimum is evaluated among positive integers K . For example, if $g < \omega_M/2$ then $K = 0$ leads to the minimum.

After setting the driving lasers in resonance with weak driving amplitudes, the Hamiltonian of the system can be approximated by the resonant part, i.e., we have $H_r \approx \tilde{H}'_r$.

4.4.2 Truncation of Hilbert Space by Using $g = g_N$

In this subsection, we show that a resonant transition described by the resonant Hamiltonian \tilde{H}'_r can be cut off by setting the optomechanical coupling strength at some specific values. Thus, we can achieve a resonant Hamiltonian that acts on a confined Hilbert space.

As shown in the resonant Hamiltonian Eq. (4.12), the matrix element coupling two resonant states is $A_{p,p'}^{(1)}\Omega_j$, which involves a Franck-Condon coefficient $A_{p,p'}^{(1)}$. Note that the Franck-Condon coefficient $A_{p,p'}^{(1)}$ is proportional to a Laguerre poly-

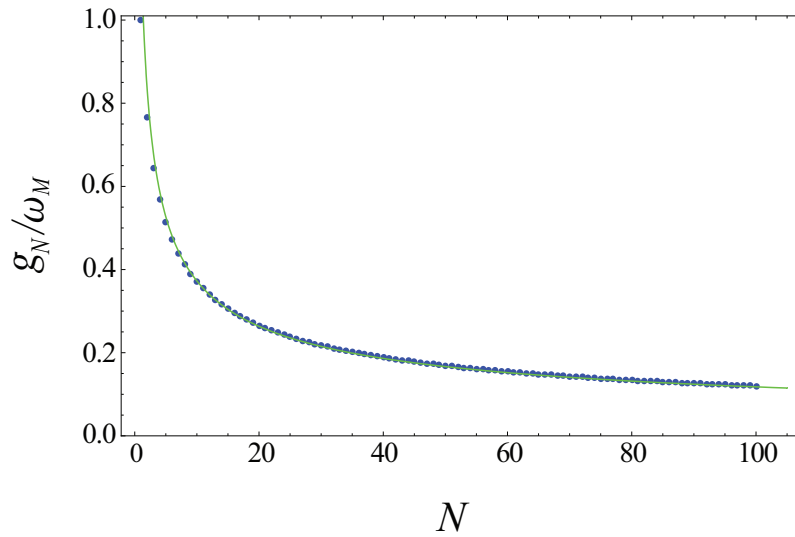


Figure 4.4: Exact solution of g_N satisfying Eq. (4.17) as a function of N (points) and result of asymptotic behavior based on Eq. (4.18)(solid line).

nomial of g/ω_M , which vanishes at some special values of g/ω_M . Therefore, we can cut off a transition from $|\psi_{0,N}\rangle$ to $|\psi_{1,N}\rangle$ by setting $A_{N,N}^{(1)} = 0$ with a special value of g . Thus, if the system is initially in the ground state, then the system can not be excited to a state with phonon number beyond N . Since the resonant Hamiltonian only involves zero- and one-photon states, so the Hilbert space becomes finite. Specifically, to have the Hamiltonian truncated within a phonon number N , we need to set the optomechanical coupling strength specifically at $g = g_N$, where g_N is the the smallest positive value to have the coefficient vanish:

$$A_{N,N}^{(1)} = \exp\left(-\frac{g_N^2}{2\omega_M^2}\right)L_N^0\left(\frac{g_N^2}{\omega_M^2}\right) = 0 \quad (4.17)$$

for a given positive integer N .

To show the specific values of g_N for different N , we plot in Fig. 4.5 the value of g_N that is the exact solution of Eq. (4.17) (points) for N from 1 to 100. We see that g_N decreases, slower and slower with larger N . In addition, we plot the values of g_N according to the asymptotic behavior of the associated Laguerre

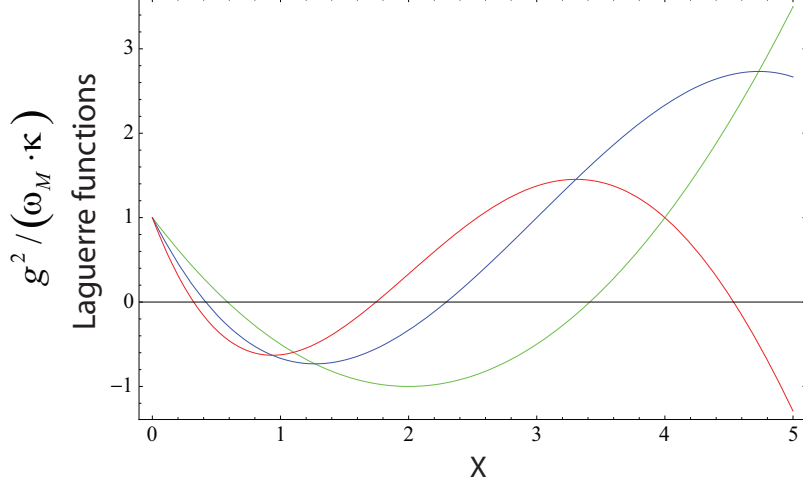


Figure 4.5: Exact solution of g_N satisfying Eq. (4.17) as a function of N (points) and result of asymptotic behavior based on Eq. (4.18)(solid line).

polynomial in the large N limit (solid line). Specifically, we obtain that

$$g_N \approx \frac{3\pi\omega_M}{8\sqrt{N}}, \quad (4.18)$$

From the Fig. 4.5, we see that Eq. (4.18) provides a good approximation for $N > 5$.

With the driving lasers satisfying the resonance condition [Eq. (4.9) and Eq. (4.10)] and the weak-driving condition [Eq. (4.16)], together with a specific optomechanical coupling strength set as $g = g_N$, we have obtained the effective Hamiltonian:

$$H_{eff} = \sum_{p=0}^{N-1} [(A_{p,p}^{(1)}\Omega_1 |\psi_{1,p}\rangle \langle\psi_{0,p}| + A_{p+1,p}^{(1)}\Omega_2 |\psi_{1,p}\rangle \langle\psi_{0,p+1}|) + H.c.], \quad (4.19)$$

which is confined in a finite subspace involving only zero- and one-photon states with phonon numbers no larger than N .

4.5 Dark States

In this section, we give an analytical form of a class of dark states based on the effective Hamiltonian in Eq. (4.19) and then study some properties of these dark

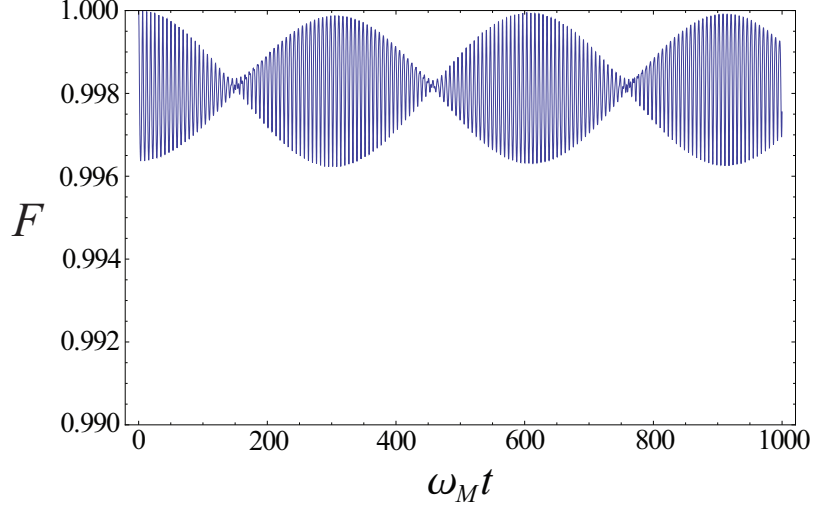


Figure 4.6: Evolution of fidelity $F = |\langle D(t)|\Psi(t)\rangle|^2$ with initial state set as a dark state. The $|\Psi(t)\rangle$ is the numerical solution of the Schrödinger equation defined by the Hamiltonian H_r . The parameters are: $g/\omega_M = 0.37$, $\Omega_1/\omega_M = 0.01$, $\Omega_2/\omega_M = 0.03$, $\Delta_1/\omega_M = -0.14$, $\Delta_2/\omega_M = -1.14$.

states. We find that the effective Hamiltonian H_{eff} has an eigenvector $|D\rangle$ with a zero eigenvalue, i.e., $H_{eff}|D\rangle = 0$. Now we give a brief derivation of the explicit form of such an eigenvector. Formally, we set the eigenvector as:

$$|D\rangle = C \sum_{p=0}^N \beta_p |p\rangle_M \otimes |0\rangle_c, \quad (4.20)$$

with C a normalization constant and β_p the coefficient of the state $|p\rangle_M \otimes |0\rangle_c$ (i.e., $|\psi_{0,p}\rangle$). Thus, the equation $H_{eff}|D\rangle = 0$ is explicitly:

$$H_{eff}|D\rangle = \sum_{p=0}^{N-1} C \left(A_{p,p}^{(1)} \Omega_1 \cdot \beta_p + A_{p+1,p}^{(1)} \Omega_2 \cdot \beta_{p+1} \right) |\psi_{1,p}\rangle = 0, \quad (4.21)$$

which reveals the fact that the excitation of a single-photon state $|\psi_{1,p}\rangle$ is a interference from two pathways: one from $|\psi_{0,p}\rangle$, the other from $|\psi_{0,p+1}\rangle$. In order to achieve a fully destructive interference such that the Eq. (4.21) is satisfied, the coefficient should obey the recurrence relation:

$$\frac{\beta_{p+1}}{\beta_p} = -\frac{\Omega_1 A_{p,p}^{(1)}}{\Omega_2 A_{p+1,p}^{(1)}}. \quad (4.22)$$

For simplicity, we set $\beta_0 = 1$. Thus, for $1 \leq p \leq N$, the coefficients are obtained:

$$\beta_p = (-1)^p \left(\frac{\Omega_1}{\Omega_2} \right)^p \prod_{i=0}^{p-1} \frac{A_{i,i}^{(1)}}{A_{i+1,i}^{(1)}}. \quad (4.23)$$

Such an eigenvector is a coherent superposition of phonon number states with the cavity field being in vacuum. In such a state, the destructive interference fully forbids excitations of cavity field even though the cavity is constantly driven by the two external fields. Therefore, it is a dark state of the optomechanical system induced by quantum coherence of the mirror. Note that in the frame where the system is governed by the Hamiltonian given in Eq. (4.6), the dark state evolves as

$$|D(t)\rangle = e^{-iH_0 t} |D\rangle = C \sum_{p=0}^N \beta_p e^{-ip\omega_M t} |p\rangle_M \otimes |0\rangle_c \quad (4.24)$$

under the approximations made in the last section.

To test the validity of the dark state as well as the effective Hamiltonian, we solve the evolution of the system state $|\Psi(t)\rangle$ based on the Schrödinger equation under the exact Hamiltonian [Eq. (4.6)] without making the approximations, i.e., $H_r |\Psi(t)\rangle = i |\dot{\Psi}(t)\rangle$. Specifically, we let the system be in a dark state initially: $|\Psi(0)\rangle = |D(0)\rangle$, and then calculate the fidelity $F = |\langle D(t) | \Psi(t) \rangle|^2$ between $|\Psi(t)\rangle$ and $|D(t)\rangle$. Given that the effective Hamiltonian H_{eff} is valid, then $|\Psi(t)\rangle$ should be well described by $|D(t)\rangle$, i.e., $F \approx 1$. We find that this is indeed the case when the condition in Eq. 4.16 is satisfied. As shown in the numerical example in Fig. 4.6, the fidelity $F > 0.99$ over a long period of time. In addition, the high frequencies patterns in Fig. 4.6 are due to off-resonant transitions, which have been ignored in H_{eff} .

Now we consider the phonon number distribution of the dark states, which is complicated by the Laguerre functions in Eq. (4.23). Although the explicit values of $|\beta_p|^2$ involve a numerical evaluation of Eq. (4.23), we find that $|\beta_p|^2$ is largely controlled by the ratio of the strengths of driving fields. Such a feature is illustrated in Fig. 4.7 (a) for various ratios of Ω_2/Ω_1 . For example, when

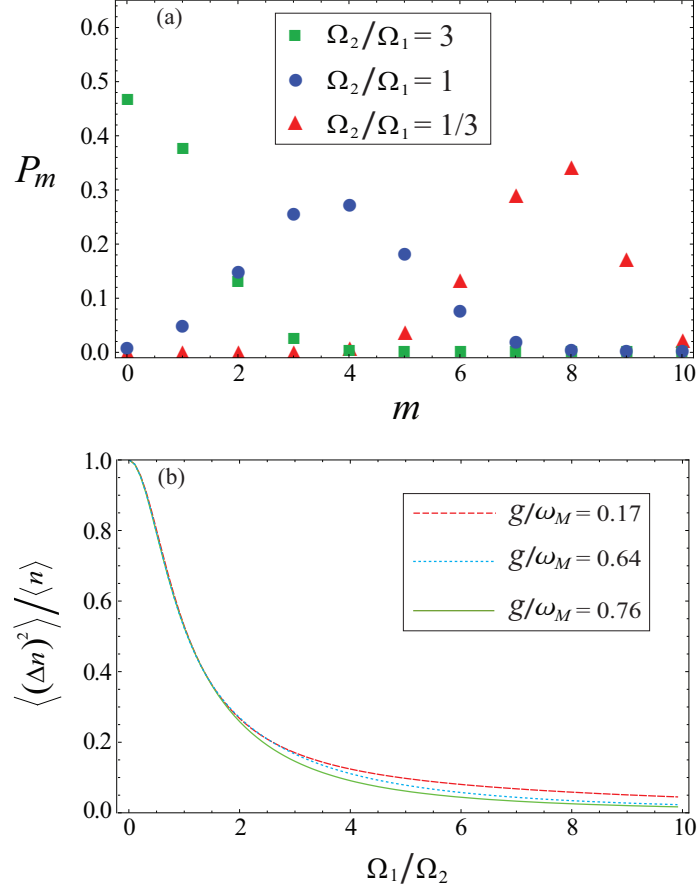


Figure 4.7: An illustration of some phonon statistics of dark states. (a) Phonon number probability distribution $P_m = |C\beta_m|^2$ of dark states for different ratios of driving strengths, with $g_N = 0.37\omega_M$ and $N = 10$. (b) $\langle(\Delta n)^2\rangle/\langle n\rangle$ as a function of Ω_1/Ω_2 for $g/\omega_M = 0.17, 0.64, 0.76$ corresponding to $N = 20, 3, 2$ respectively.

$\Omega_2/\Omega_1 = 3$, the probability P_m of m th mirror Fock state decreases quickly with phonon number m . However, when the ratio becomes $\Omega_2/\Omega_1 = 1$, a peak appears in the probability distribution. Moreover, when the ratio further decreases to $\Omega_2/\Omega_1 = 1/3$, the peak is shifted towards higher phonon numbers.

In order to further study the statistical property of the distributions, we plot in Fig. 4.7 (b) the ratio $\langle(\Delta n)^2\rangle/\langle n\rangle$ as a function of Ω_1/Ω_2 , which shows that phonon number distributions of dark states exhibit a sub-Poissonian statistics. One can see that $\langle(\Delta n)^2\rangle/\langle n\rangle$ decreases with Ω_1/Ω_2 and is always less than 1

(i.e., sub-Poisson distribution) except for the small region Ω_1/Ω_2 near zero. Additionally, we find that the curves are quite insensitive to different values of g_N .

Here we make a theoretical analysis on the influence of small deviation of g_N to the dark states. Note that the specific optomechanical coupling strength g_N has been used in order to obtain the effective Hamiltonian H_{eff} applicable to mirror states of phonon numbers in the range $0 \leq p \leq N$. When $g \neq g_N$, $A_{N,N}^{(1)}$ is nonzero, then the Hamiltonian cannot be exactly truncated. Let us consider the system with g slightly deviated from g_N , if the initial state is a dark state $|D\rangle$, then the system will make a transition to $|1\rangle_c |\tilde{N}\rangle_M$ by the driving field of frequency ω_1 , and subsequent interactions with the driving fields could excite the mirror to phonon number states higher than N . However, we point out that since the transition rate from to $|1\rangle_c |\tilde{N}\rangle_M$ is proportional to $|\beta_N|^2 \times |A_{N,N}^{(1)}|^2$ according to first order perturbation theory, the transition probability out of $|D\rangle$ would be negligible in a finite time duration as long as the product of $|\beta_N|^2$ and $|A_{N,N}^{(1)}|^2$ is sufficiently small. If such a condition is satisfied, then $|D\rangle$ may still be treated as a dark state approximately even though g is slightly deviated from g_N . Indeed, as we have illustrated the phonon number distribution of $|D\rangle$ in Fig. 4.7 (a), $|\beta_N|^2$ can be highly suppressed by using $\Omega_2 > \Omega_1$, such that the dark state can still be valid with small deviation of g from g_N .

4.6 Preparation of Dark States by Optical Pumping

In this section, we study how the system can be optically pumped into the dark states in presence of cavity-field damping. In the frame where the system Hamiltonian is given by Eq. (4.6), the evolution of the system under cavity field damping is governed by the master equation:

$$\frac{d\rho}{dt} = -i[H_r, \rho] - \frac{\kappa}{2} (a^\dagger a \rho - 2a \rho a^\dagger + \rho a^\dagger a), \quad (4.25)$$

where ρ is the density matrix of the optomechanical system, and κ is the cavity-field damping rate. Note that the mechanical dissipation is not included in the master equation (4.25). The ignorance of mechanical damping can be justified if the mechanical damping rate γ_M is much smaller than κ and the time interval of interest is restricted to $t \ll 1/\gamma_M$. In particular, there is a time interval $\kappa^{-1} \ll t \ll \gamma_M^{-1}$ where the optically pumping is almost completed before the mechanical dissipation becomes significant. To support our arguments, we will also discuss the effect of mechanical damping on the dark state preparation later.

First of all, we note that if the approximation $H'_r \approx H_{eff}$ is perfect, then by going back to the original frame governed by the system Hamiltonian H_r in Eq. (4.6), $\rho = |D(t)\rangle\langle D(t)|$ is already a solution of the master equation Eq. (4.25). This is because cavity field is in vacuum in the dark states, such that the cavity field damping has no effect on $|D\rangle$ (which has zero photon) at all. However, we use the exact Hamiltonian H_r instead of H_{eff} in the master equation so as to study the evolution of the system without relying on the approximations.

The master equation Eq. (4.25) is equivalent to a set of coupled ordinary differential equations, which can be solved numerically with an initial ground state of the system. To perform numerical calculations, we truncate the dimension of the density matrix, which is sufficiently larger than that of the dark state density matrix. For the parameters used in the figures in this section, $\rho(t)$ appears to be converging when the photon and phonon number states are kept up to 2 and 15 respectively. In particular, we are interested in the fidelity F defined by

$$F = \text{Tr} (|D(t)\rangle\langle D(t)| \rho(t)), \quad (4.26)$$

which represents the probability of the system in the dark state. In Fig. 4.8, the preparations of the dark states by optical pumping are demonstrated in various cases. It is shown that the fidelity F increases with time and gradually approaches a steady value close to 1. For the three cases shown in Fig. 4.8, the fidelities can reach $F \approx 0.99$ with $g_N/\omega_M = 0.37$ ($N = 10$) at the time $T \approx 8000\omega_M^{-1}$.

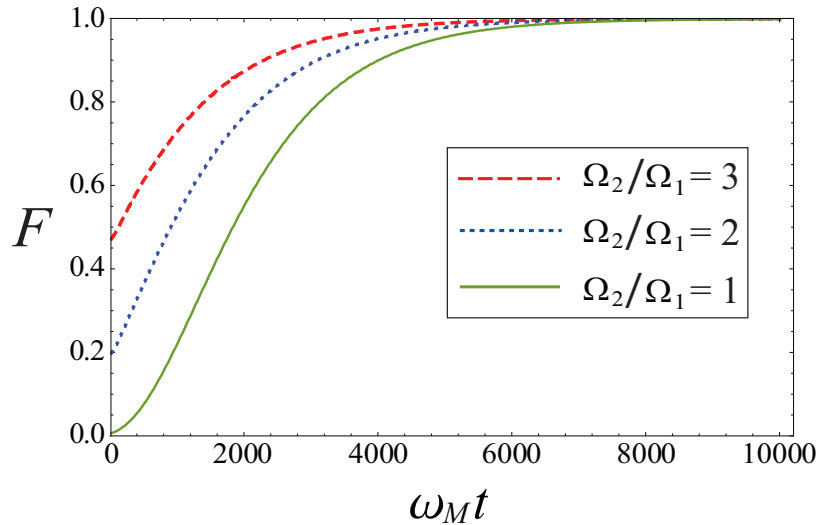


Figure 4.8: Preparation of dark states by optical pumping. The fidelities F for various Ω_2/Ω_1 ratios are plotted as a function of time. The parameters are: $g_N/\omega_M = 0.37$, $N = 10$, $\kappa/\omega_M = 0.05$, $\Omega_2/\omega_M = 0.01$, $\Delta_1/\omega_M = -0.14$, $\Delta_2/\omega_M = -1.14$.

Such a scheme of preparing dark states indeed shares the same principle as optical pumping to a certain atomic states in atomic physics. Specifically, the increase of F is understood because when a photon leaks out of the cavity, the mirror always has a non-zero transition probability going to the dark state. Since the dark state is decoupled from the driving fields, it can no longer be excited, and hence the occupation of the dark state accumulates as time increases. However, we remark that during the optical pumping process, there is a loss due to the cavity field decay, which makes the mirror make a transition to phonon number states higher than N . But such a loss, which amounts to about 1% in Fig. 4.8, can be reduced if N is chosen to be large enough.

In the previous section, we have analyzed that if g is slightly deviated from g_N , then the quantity $|\beta_N|^2 \times |A_{N,N}^{(1)}|^2$ would characterize the degradation of $|D\rangle$ as a dark state. This is because this quantity is proportional to the probability leakage rate out of the state $|D\rangle$ when $g \neq g_N$. In addition, we have pointed out

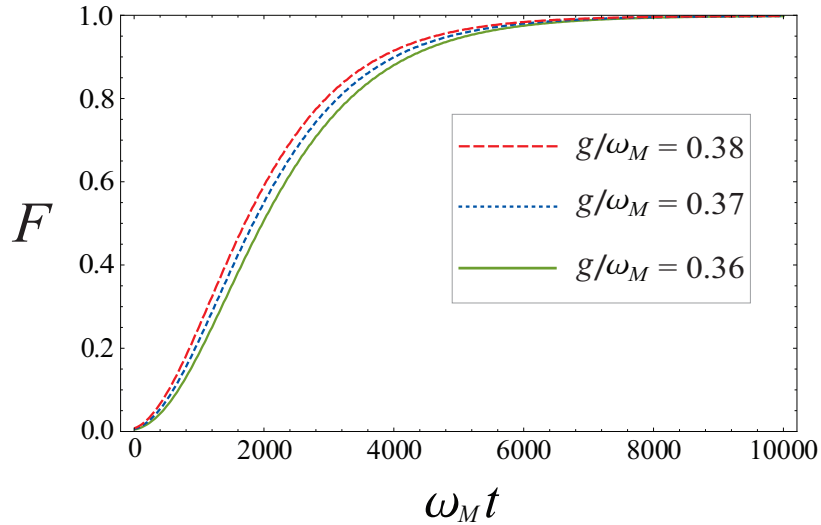


Figure 4.9: Time evolution of the fidelities F for various g in the vicinity of $g_N = 0.37\omega_M$. The parameters are: $\kappa/\omega_M = 0.05$, $\Omega_1 = \Omega_2 = 0.01\omega_M$, $\Delta_1/\omega_M = -0.14$, $\Delta_2/\omega_M = -1.14$.

that a large ratio between driving strengths Ω_2/Ω_1 can make $|\beta_N|^2$ insignificant for N th Fock state, which is at the boundary of the dark state. Such a effect of small deviations of g can be revealed in the dark states preparation process. We have tested numerically the sensitivity of dark states fidelity to small variations of g values when $\Omega_2 \geq \Omega_1$. In particular, we provide an example in Fig. 4.9, which shows that the fidelities still reach about $F \approx 0.99$ in presence of about 3% deviations from the g_N value. Such results suggests that dark state preparation is indeed insensitive to small variations of g values.

Now we consider the influence of mechanical damping on preparation of the dark states. Generally, mechanical damping leads to the decoherence of the quantum state of the mirror, thus damaging the preparation of dark states. To quantify such influence, we take into account the mechanical damping into the master

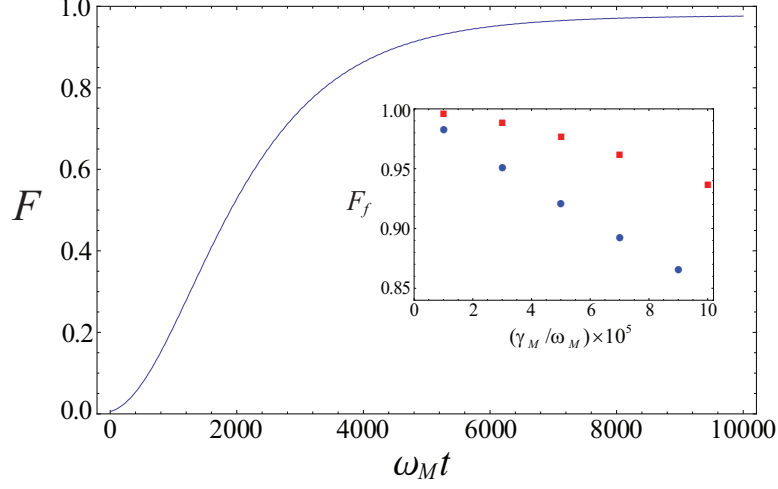


Figure 4.10: Evolution of fidelity F for a mechanical damping rate $\gamma_M/\omega_M = 5 \times 10^{-5}$ and thermal phonon number $\bar{n}_M = 0$. The inset figure shows the final fidelity F_f (at $\omega_M t = 10^4$) for various γ_M , with thermal phonon numbers are $\bar{n}_M = 0$ (red squares) and $\bar{n}_M = 1$ (blue circles). The parameters are: $g/\omega_M = 0.37$, $\kappa/\omega_M = 0.05$, $\Omega_1 = \Omega_2 = 0.01\omega_M$, $\Delta_1/\omega_M = -0.14$, $\Delta_2/\omega_M = -1.14$.

equation:

$$\begin{aligned} \frac{d\rho}{dt} = & -i[H_r, \rho] - \frac{\kappa}{2} (a^\dagger a \rho - 2a\rho a^\dagger + \rho a^\dagger a) - \frac{\gamma_M(\bar{n}_M + 1)}{2} (b^\dagger b \rho - 2b\rho b^\dagger + \rho b^\dagger b) \\ & - \frac{\gamma_M \bar{n}_M}{2} (bb^\dagger \rho - 2b^\dagger \rho b + \rho bb^\dagger), \end{aligned} \quad (4.27)$$

where γ_M is the mechanical damping rate, \bar{n}_M is the thermal average phonon number, and we have assumed that the damping is due to the coupling to a Markovian bath.

We solve the master equation numerically and plot in Fig. 4.10 the evolution of fidelity with a mechanical damping rate $\gamma_M/\omega_M = 5 \times 10^{-5}$, while the other parameters and size of Hilbert space are the same to the case of the green curve in Fig. 4.8. It is shown that the fidelity grows to about 0.97 finally, which is slightly lower than that of Fig. 4.8. Such a result indicates that, a mechanical damping at this magnitude has a small influence to the preparation of dark states. Moreover, we provide the dependence of final dark state fidelity on the mechanical damping

rate for thermal phonon numbers $\bar{n}_M = 0$ and $\bar{n}_M = 1$ respectively in the inset figure, which shows that final fidelity declines as the mechanical damping rate increases and average thermal phonon number increases. Hence, a mechanical damping rate $\gamma_M/\omega_M < 10^{-4}$ is essential to successful preparation of dark state at the time scale of $\omega_M t = 10^4$. In other words, the life time of the phonons should be longer than the time interval of dark states preparation.

4.7 Conclusion

In conclusion, we have addressed a quantum interference effect in the single-photon strong-coupling regime of cavity optomechanics. In such a regime, we discover a class of dark states of a moving mirror that are coherent superpositions of mirror Fock states, under the conditions [Eq. (4.9), Eq. (4.10), Eq. (4.16)]. In Particular, for dark states involving N mirror Fock states with $N < 20$ as we have explored, we require a strong single-photon coupling strength g that is comparable to the mechanical frequency ω_M , and the cavity field decay rate κ should be much smaller than ω_M so as to achieve resolved sidebands. In such dark states, the cavity field remains in vacuum state though driven by two external fields, and this is due to a quantum destructive interference effect. In other words, the cavity field is decoupled from two driving fields. An analytical expression of the dark states is provided, which indicates the dependence of phonon number distribution on the ratio of the driving amplitudes Ω_2/Ω_1 and the optomechanical coupling strength g . In addition, numerical calculations show that phonon number distributions of the dark states exhibit sub-Poissonian statistics. Furthermore, we demonstrate that the dark states can be prepared with high fidelity by optical pumping. In particular, our numerical simulations indicate that such preparation of the dark states is insensitive to small deviations of g values if $\Omega_2 \geq \Omega_1$, and the effect of mechanical damping is negligible when the lifetime of phonons is longer than the

preparation time.

We note that in literature, there is a related study on a different type of dark states phenomena in two-mode optomechanical systems by Hailin Wang and coworkers [33]. Their type of dark states is termed optomechanical dark mode, which is a coherent superposition of two optical modes of the cavity field. It is claimed that when the cavity field is set in such a dark mode, then the mechanical oscillator and the cavity field will be decoupled from each other. However, the cavity field is still coupled to the external driving fields, such that the cavity contains a number of photons. On the contrary, our type of dark states involve coherent superpositions of mechanical number states and exist in a single-mode cavity. Moreover, in our dark states the cavity is decoupled from external fields and contains no photons. Hence, our type of dark states is different from the optomechanical dark mode, even though both involve quantum interference effects. We also remark that the optomechanical dark mode exists in the weak coupling regime and is experimentally observed by Hailin Wang and coworkers.

Chapter 5

Optomechanical Cavity with an Atom: an Effective Atom-mirror Coupling

5.1 Introduction

In this chapter, we investigate an effective coupling between a two-level atom and a mesoscopic mechanical oscillator mediated by an optical field. Such a coupling implies a possible scheme of quantum state transfer between the atom and mechanical oscillator. With the help of well developed techniques in atomic physics, such a state transfer can be used to prepare, manipulate and detect the quantum state of a mesoscopic mechanical oscillator. In literature of optomechanics, there have been various schemes of state transfers between a Bose-Einstein condensate and an optomechanical mirror [89], cavity photons and phonons [8, 90], a solid state qubit and photons [?], as well as two different cavity field modes [73, 91], which are aimed at possible applications of cavity optomechanical system in quantum information. In addition, there is a closely related study on the coupling between the spatial motions of a single atom and a mechanical oscillator

[92].

For an optomechanical cavity with a fixed atom inside, the cavity field interacts with both the atom and the moving mirror, such that the cavity field can serve as a medium for an indirect coupling between the atom and the mirror. Our task is to achieve a coupling between the atom and mirror effectively, exhibiting a Rabi oscillation:

$$|\Psi(t)\rangle = \cos\omega t |g\rangle |0\rangle_M \otimes |0\rangle_C - i \sin\omega t |e\rangle |1\rangle_M \otimes |0\rangle_C, \quad (5.1)$$

where an atomic excitation is accompanied by an excitation of a phonon, while the cavity field is kept in the vacuum state. Such an oscillation leads to a full atom-mirror entanglement and quantum state transfer scheme between the atom and the mirror.

5.2 The Model

We investigate an optomechanical system formed by an optical cavity with one harmonically bounded end mirror and a two-level atom inside, where the movable end mirror and the atom are coupled to cavity field separately. Additionally, the cavity is externally driven by a laser with a frequency ω_L and an amplitude Ω (Fig. 5.1). The Hamiltonian of such a driven system under RWA is

$$H = \omega_C a^\dagger a + \omega_M b^\dagger b + \omega_A \sigma_{ee} - g a^\dagger a (b^\dagger + b) + G \sigma_{ge} a^\dagger + G \sigma_{eg} a + \Omega e^{-i\omega_L t} a^\dagger + \Omega^* e^{i\omega_L t} a, \quad (5.2)$$

where a (b) and ω_c (ω_M) are respectively the annihilation operator and resonant frequency of the cavity field (mechanical) modes, and we have set $\hbar = 1$. The frequency ω_A is the energy difference between the excited state $|e\rangle$ and ground state $|g\rangle$ of the atom, and $\sigma_{ij} = |i\rangle \langle j|$ with $|i\rangle$ and $|j\rangle$ denoting states of the atom. The parameters g and G are respectively, the mirror-photon and atom-photon coupling strengths. Specifically, the atom-photon coupling strength is

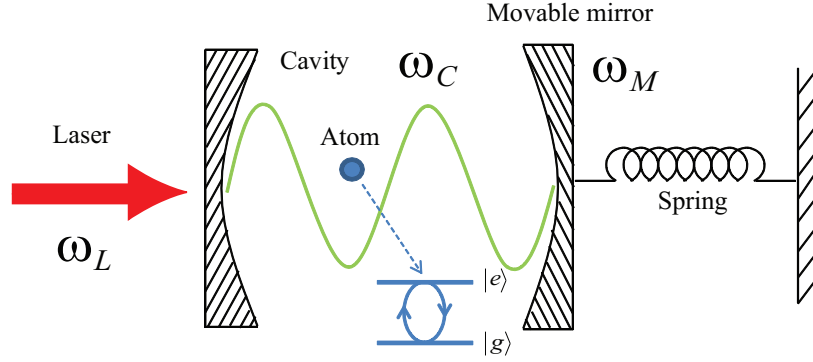


Figure 5.1: Schematic diagram of an optomechanical system with a two-level atom inside, driven by an external field.

given by $G = i\sqrt{\frac{\hbar\omega_C}{2\varepsilon_0}}\vec{d}_{ge} \cdot \vec{f}_C(\vec{r}_0)$, where $\vec{f}_C(\vec{r}_0)$ is the cavity field mode function at the atom position \vec{r}_0 , and $\vec{d}_{ge} = \langle g|\vec{d}|e\rangle$ is an element of dipole moment. By appropriately choosing the phases of atomic states, we set G as real.

To eliminate the time-dependence of the Hamiltonian, we go to a rotating frame, where the Hamiltonian becomes

$$H' = \Delta_C a^\dagger a + \omega_M b^\dagger b + \Delta_A \sigma_{ee} - ga^\dagger a (b^\dagger + b) + G\sigma_{ge} a^\dagger + G\sigma_{eg} a + \Omega a^\dagger + \Omega^* a, \quad (5.3)$$

where we have defined the detunings $\Delta_C = \omega_C - \omega_L$ and $\Delta_A = \omega_A - \omega_L$. As has been discussed in chapter 2.3, the Hamiltonian H_0 of the optomechanical system without driving can be diagonalized as

$$H_0 = \Delta_C a^\dagger a + \omega_M b^\dagger b - ga^\dagger a (b^\dagger + b) = \sum_{n,p} \varepsilon_{n,p} |\psi_{n,p}\rangle \langle \psi_{n,p}|. \quad (5.4)$$

where $|\psi_{n,p}\rangle = |n\rangle_C \otimes |\tilde{p}\rangle_M$ are eigenvectors with energy eigenvalues $\varepsilon_{n,p} = n\Delta_C + p\omega_M - n^2g^2/\omega_M$ and $|\tilde{p}\rangle_M$ are displaced number states of the mirror. In such a basis, the Hamiltonian of the system takes an alternative form:

$$\begin{aligned} H' = & \sum_{n,p} \varepsilon_{n,p} |\psi_{n,p}\rangle \langle \psi_{n,p}| + \Delta_A |e\rangle \langle e| + \sum_{n,p,p'} \left[A_{p,p'}^{(n)} G \sigma_{ge} |\psi_{n,p'}\rangle \langle \psi_{n-1,p}| + h.c. \right] \\ & + \sum_{n,p,p'} \left[A_{p,p'}^{(n)} \Omega |\psi_{n,p'}\rangle \langle \psi_{n-1,p}| + h.c. \right], \end{aligned} \quad (5.5)$$

in which the quantum transitions due to the atom-field coupling and external driving are specified and the nonlinear optomechanical coupling is diagonalized. As a result, there are only two coupling channels in this basis, rather than three channels in the Fock state basis, thus leading to the simplicity in analyzing the dynamics of the system. The energy level structure of the system is shown in Fig. 5.2 (a).

5.3 Effective Two-level Hamiltonian

In this section, we show that under certain resonance and large detuning conditions, we can achieve an effective two-level Hamiltonian that involves only the ground state $|\psi_{0,0}\rangle |g\rangle$ ($|0\rangle_C |0\rangle_M |g\rangle$) and an excited state $|\psi_{0,1}\rangle |e\rangle$ ($|0\rangle_C |1\rangle_M |e\rangle$).

The driven system can be captured by a Λ -type three-level system involving the states: $|\psi_{0,0}\rangle |g\rangle$, $|\psi_{0,1}\rangle |e\rangle$ and $|\psi_{1,0}\rangle |g\rangle$ ($|1\rangle_C |\tilde{0}\rangle_M |g\rangle$), as shown in Fig. 5.2. The key is to specifically set the laser driving frequency ω_L , such that the transition from $|\psi_{0,0}\rangle |g\rangle$ to $|\psi_{1,0}\rangle |g\rangle$ is detuned by Δ_2 , while the combined excitation from $|\psi_{0,0}\rangle |g\rangle$ to $|\psi_{0,1}\rangle |e\rangle$ is in resonance, i.e., a Raman resonance between these two states is established. Together with the weak coupling strengths Ω and G , we obtain a three-level system [Fig. 5.2 (b)] with the Hamiltonian

$$\begin{aligned}
 H_\Lambda = & \Delta_2 \sigma_{gg} |\psi_{1,0}\rangle \langle \psi_{1,0}| + \Delta_3 \sigma_{ee} |\psi_{0,1}\rangle \langle \psi_{0,1}| \\
 & + (A_{0,0} \Omega \sigma_{gg} |\psi_{1,0}\rangle \langle \psi_{0,0}| + A_{1,0} G \sigma_{ge} |\psi_{1,0}\rangle \langle \psi_{0,1}| + h.c.), \quad (5.6)
 \end{aligned}$$

where we have introduced two detunings: $\Delta_2 = \omega_C - \omega_L - g^2/\omega_M$, and $\Delta_3 = \omega_A - \omega_L + \omega_M$; and we denote $A_{i,j} = A_{i,j}^{(1)}$ for simplicity. Δ_2 is the detuning of a transition from the ground state to the intermediate state, while Δ_3 represents the detuning of the Raman transition between $|\psi_{0,0}\rangle |g\rangle$ and $|\psi_{0,1}\rangle |e\rangle$. Thus, the large detuning and weak driving condition is explicitly

$$\Omega \ll \Delta_2, G \ll \Delta_2. \quad (5.7)$$

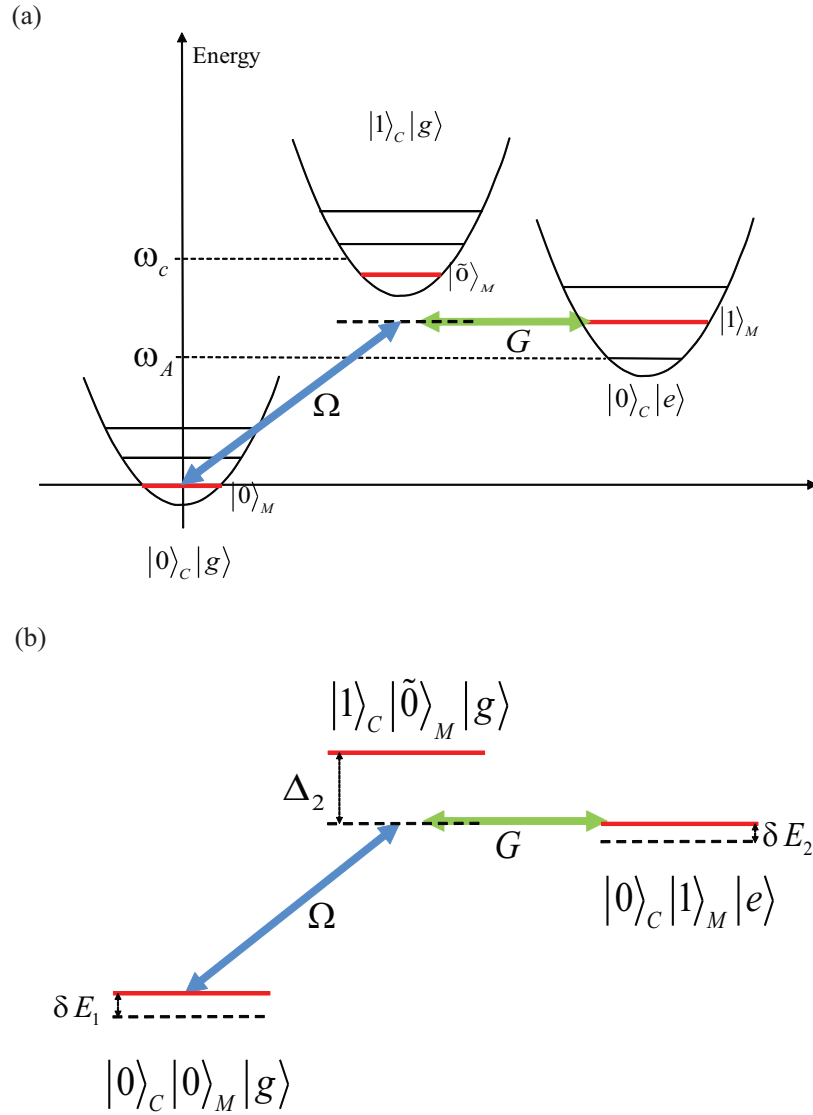


Figure 5.2: (a) Energy-level structure of the atom assisted optomechanical system, driven by an external field. (b) Scheme of the Λ type three-level model under the large detuning and resonance conditions.

In addition, to have a near resonant Raman transition, we also require $|\Delta_3| \ll |\Delta_2|$.

For such a three-level system, the intermediate state $|\psi_{1,0}\rangle|g\rangle$ can be effectively eliminated under the condition in Eq. (5.7) such that the system is modeled by a two-level Hamiltonian. To see this, we let the state of the system be:

$$|\Psi(t)\rangle = c_1(t)|\psi_{0,0}\rangle|g\rangle + c_2(t)|\psi_{1,0}\rangle|g\rangle + c_3(t)|\psi_{0,1}\rangle|e\rangle. \quad (5.8)$$

Therefore, the Schrödinger equation defined by the three-level Hamiltonian in Eq. (5.6) yields

$$i\dot{c}_1(t) = A_{0,0}\Omega^*c_2(t), \quad (5.9)$$

$$i\dot{c}_2(t) = \Delta_2c_2(t) + A_{0,0}\Omega c_1(t) + A_{1,0}Gc_3(t), \quad (5.10)$$

$$i\dot{c}_3(t) = \Delta_3c_3(t) + A_{1,0}Gc_2(t). \quad (5.11)$$

Under the large detuning and weak driving condition that $\Omega \ll \Delta_2, G \ll \Delta_2$, one can make the adiabatic approximation that $\dot{c}_2(t) \approx 0$. According to Eq. (5.10), the amplitude of the intermediate state is approximately

$$c_2(t) \approx -\frac{1}{\Delta_2} [A_{0,0}\Omega c_1(t) + A_{1,0}Gc_3(t)], \quad (5.12)$$

which is much smaller than 1 due to the large detuning and weak driving condition. Therefore, the equations of motion reduce to

$$i\dot{c}_1(t) = -\frac{A_{0,0}\Omega^*}{\Delta_2} [A_{0,0}\Omega c_1(t) + A_{1,0}Gc_3(t)], \quad (5.13a)$$

$$i\dot{c}_3(t) = \Delta_3c_3(t) - \frac{A_{1,0}G}{\Delta_2} [A_{0,0}\Omega c_1(t) + A_{1,0}Gc_3(t)], \quad (5.13b)$$

which only involve the ground state and the third state. Eq. (5.13) implies an effective Hamiltonian that governs the evolution of these two states:

$$\begin{aligned} H_{eff} = & -\frac{|A_{0,0}\Omega|^2}{\Delta_2} \sigma_{gg} |\psi_{0,0}\rangle \langle \psi_{0,0}| + (\Delta_3 - |A_{1,0}G|^2/\Delta_2) \sigma_{ee} |\psi_{0,1}\rangle \langle \psi_{0,1}| \\ & + \left(-\frac{A_{0,0}\Omega A_{1,0}G}{\Delta_2} \sigma_{eg} |\psi_{0,1}\rangle \langle \psi_{0,0}| - \frac{A_{0,0}\Omega^* A_{1,0}G}{\Delta_2} \sigma_{ge} |\psi_{0,0}\rangle \langle \psi_{0,1}| \right). \end{aligned} \quad (5.14)$$

Hence, exact resonance between the two states requires the detuning Δ_3 be:

$$\Delta_3 = (|A_{1,0}G|^2 - |A_{0,0}\Omega|^2) / \Delta_2. \quad (5.15)$$

Now we go to a frame rotating at the frequency $-|A_{0,0}\Omega|^2 / \Delta_2$, such that the effective two-level Hamiltonian takes a neat form:

$$H_{eff} = \Omega_{eff}\sigma_{eg} |\psi_{0,1}\rangle \langle \psi_{0,0}| + \Omega_{eff}^*\sigma_{ge} |\psi_{0,0}\rangle \langle \psi_{0,1}|, \quad (5.16)$$

with

$$\Omega_{eff} = -A_{0,0}A_{1,0}\Omega G / \Delta_2 \quad (5.17)$$

being the effective driving strength.

Here we discuss the single-photon optomechanical coupling strength g required for the effective Hamiltonian. The coupling strength g is related to the magnitude of the effective driving strength, because the Franck-Condon factors $A_{0,0}$ and $A_{1,0}$ are determined by g according to Eq. (3.4). Explicitly, we have $A_{0,0}A_{1,0} = \xi e^{-\xi^2}$ with $\xi = g/\omega_M$. To show such a dependence directly, we plot in Fig. 5.3 the product $A_{0,0}A_{1,0}$ as a function of g/ω_M . We see that $A_{0,0}A_{1,0}$ increases from zero at $g/\omega_M = 0$ and reaches a peak at about $g/\omega_M = 0.8$, then declines gradually and approaches to zero in the large g limit. In particular, there is a region roughly $0.1\omega_M < g < 1.5\omega_M$ to have a significant magnitude of the product $A_{0,0}A_{1,0}$ above 0.1. Note that a sufficiently large effective driving strength is needed in order to have the coherent evolution process overwhelms all kinds of dissipations. Hence, an appropriate optomechanical coupling strength g in the single-photon strong coupling regime is required to have a significant effective driving strength Ω_{eff} , such that the dynamical evolution of the system is modeled by the effective Hamiltonian [Eq. (5.16)].

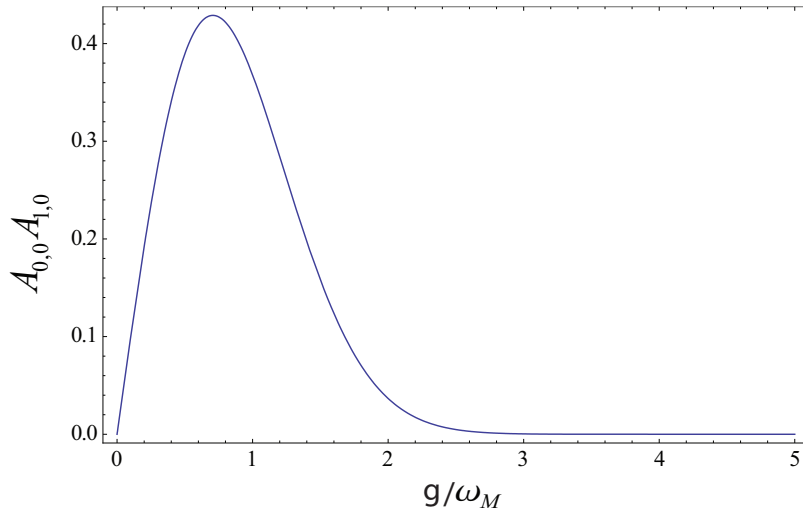


Figure 5.3: The product of Franck-Condon factors $A_{0,0}A_{1,0}$ as a function of g/ω_M .

5.4 Improvement of the Two-level Model

In the previous section, we have kept only $|\psi_{1,0}\rangle|g\rangle$ and neglected the effects of states $|\psi_{1,r}\rangle|g\rangle$ ($r \geq 1$) as intermediate states. In order to improve the model, we need to include $|\psi_{1,r}\rangle|g\rangle$ states into the equations before the adiabatic elimination procedure is performed. As we shall see below, the intermediate states $|\psi_{1,r}\rangle|g\rangle$ have very small population but they can generate an appreciable energy shift.

Let the state of the system (initially in ground state $|\psi_{0,0}\rangle|g\rangle$) be

$$|\Psi(t)\rangle = a_0(t)|\psi_{0,0}\rangle|g\rangle + b_1(t)|\psi_{0,1}\rangle|e\rangle + \sum_{r=0}^N c_r(t)|\psi_{1,r}\rangle|g\rangle + \sum_s d_s(t)|\psi_{1,s}\rangle|e\rangle, \quad (5.18)$$

where $a_0(t)$, $b_1(t)$, $c_r(t)$ and $d_s(t)$ are respectively the time-dependent coefficients of $|\psi_{0,0}\rangle|g\rangle$, $|\psi_{0,1}\rangle|e\rangle$, $|\psi_{1,r}\rangle|g\rangle$ and $|\psi_{1,s}\rangle|e\rangle$. According to the Schrödinger equa-

tion $i|\dot{\Psi}(t)\rangle = H'|\Psi(t)\rangle$, the equations of motion for the coefficients are obtained

$$i\dot{a}_0(t) = \varepsilon_{0,0}a_0(t) + \sum_{r=0}^N A_{0,r}^{(1)}\Omega^*c_r(t), \quad (5.19)$$

$$i\dot{b}_1(t) = (\varepsilon_{0,1} + \omega_A - \omega_L)b_1(t) + \sum_{r=0}^N A_{1,r}^{(1)}Gc_r(t) + \sum_s A_{1,s}^{(1)}\Omega^*d_s(t), \quad (5.20)$$

$$i\dot{c}_r(t) = \varepsilon_{1,r}c_r(t) + A_{0,r}^{(1)}\Omega a_0(t) + A_{1,r}^{(1)}Gb_1(t), \quad (5.21)$$

$$i\dot{d}_s(t) = (\varepsilon_{1,s} + \omega_A - \omega_L)d_s(t) + A_{1,s}^{(1)}\Omega b_1(t). \quad (5.22)$$

In the large detuning limit, we again have $\dot{c}_r(t) \approx 0$, $\dot{d}_s(t) \approx 0$, such that we obtain the relations

$$d_s(t) = -\frac{A_{1,s}^{(1)}\Omega}{\varepsilon_{1,s} + \omega_A}b_1(t), \quad (5.23)$$

$$c_r(t) = -\frac{1}{\varepsilon_{1,r}}\left(A_{0,r}^{(1)}\Omega a_0(t) + A_{1,r}^{(1)}Gb_1(t)\right). \quad (5.24)$$

Therefore, the equations of motion reduce to

$$i\dot{a}_0 = \left(\varepsilon_{0,0} - \sum_r \frac{|A_{0,r}^{(1)}\Omega|^2}{\varepsilon_{1,r}}\right)a_0(t) - \sum_r \frac{A_{0,r}^{(1)}\Omega^*A_{1,r}^{(1)}G}{\varepsilon_{1,r}}b_1(t), \quad (5.25)$$

$$i\dot{b}_1(t) = \left(\Delta_3 - \sum_r \frac{|A_{1,r}^{(1)}G|^2}{\varepsilon_{1,r}} - \sum_s \frac{|A_{1,s}^{(1)}\Omega|^2}{\Delta_2 + \Delta_3 + (s-1)\omega_M}\right)b_1(t) - \sum_r \frac{A_{1,r}^{(1)}GA_{0,r}^{(1)}\Omega}{\varepsilon_{1,r}}a_0(t), \quad (5.26)$$

in which the states $|\psi_{0,0}\rangle |g\rangle$ and $|\psi_{0,1}\rangle |e\rangle$ are coupled effectively, and $\Delta_3 = \omega_A + \omega_M - \omega_L$ is defined. We interpret Eq. (5.25) and (5.26) as the Schrödinger equation governed by an effective Hamiltonian, which can be expressed in matrix form as

$$H_{eff} = \left[\begin{array}{cc} \left(\varepsilon_{0,0} - \sum_r \frac{|A_{0,r}^{(1)}\Omega|^2}{\varepsilon_{1,r}}\right) & -\sum_r \frac{A_{0,r}^{(1)}\Omega^*A_{1,r}^{(1)}G}{\varepsilon_{1,r}} \\ -\sum_r \frac{A_{1,r}^{(1)}GA_{0,r}^{(1)}\Omega}{\varepsilon_{1,r}} & \left(\Delta_3 - \sum_r \frac{|A_{1,r}^{(1)}G|^2}{\varepsilon_{1,r}} - \sum_s \frac{|A_{1,s}^{(1)}\Omega|^2}{\Delta_2 + \Delta_3 + (s-1)\omega_M}\right) \end{array} \right], \quad (5.27)$$

which describes the interaction of the two-level system. Particularly, we are interested in the case where the two states are in resonance, with the resonance

condition given by

$$\Delta_3 = \sum_r \left(\frac{|A_{1,r}^{(1)}G|^2 - |A_{0,r}^{(1)}\Omega|^2}{\Delta_2 + r\omega_M} + \frac{|A_{1,r}^{(1)}\Omega|^2}{\Delta_2 + (r-1)\omega_M} \right), \quad (5.28)$$

where we have used the relations: $\varepsilon_{0,0} = 0$ and $\varepsilon_{1,r} = \Delta_2 + r\omega_M$. Besides, we have taken an approximation based on $|\Delta_3| \ll |\Delta_2|$. Note that this resonance condition is different from the one [Eq. (5.15)] derived in the previous section. The extra summation terms in Eq. (5.28) result from the off-resonant couplings of the two states $|\psi_{0,0}\rangle|g\rangle$ and $|\psi_{0,1}\rangle|e\rangle$ with the serials of states $|\psi_{1,r}\rangle|g\rangle$ and $|\psi_{1,s}\rangle|e\rangle$. Such off-resonant couplings have an effect of causing energy shifts to the two states $|\psi_{0,0}\rangle|g\rangle$ and $|\psi_{0,1}\rangle|e\rangle$, leading to the modification of the resonance condition. In addition, we obtain the effective driving strength in this improved model:

$$\Omega'_{eff} = - \sum_r \frac{A_{1,r}^{(1)}GA_{0,r}^{(1)}\Omega}{\varepsilon_{1,r}}, \quad (5.29)$$

which is different from the previous one in Eq. (5.17).

Hence, we have shown that under large detuning and resonant condition, an effective coupling between the ground state and an excited state can be achieved. We remark that, the excited state can be set as any state $|\psi_{0,q}\rangle|e\rangle$ with $q = 0, 1, 2, \dots$ by adjusting the laser frequency ω_L according to separate the resonance condition. Here we choose $|\psi_{0,1}\rangle|e\rangle$ to be the excited state as an representative example, which contains general features as we will discuss later.

5.5 Atom-mirror Rabi Oscillations

Let the system be prepared in the ground state initially, i.e., $|\Psi(0)\rangle = |g\rangle|0\rangle_M \otimes |0\rangle_C$. According to the effective two-level Hamiltonian, the time evolution of the system reads

$$|\Psi(t)\rangle = \cos(|\Omega_{eff}|t) |g\rangle|0\rangle_M \otimes |0\rangle_C - i \sin(|\Omega_{eff}|t) |e\rangle|1\rangle_M \otimes |0\rangle_C, \quad (5.30)$$

which exhibits itself as a typical Rabi oscillation with a probability oscillation period $T = \pi/|\Omega_{eff}|$.

In order to explore the performance of the above model and test whether such Rabi oscillations exist under the conditions, we now turn to numerical simulations of coherent evolution of the system under the exact Hamiltonian [Eq. (5.3)] without making the approximations in Sec.3 and Sec. 4. We solve numerically the Schrödinger equation governed by this Hamiltonian under the resonance condition [Eq. (5.28)] with a Hilbert space truncated at largest photon number 2 and largest phonon number 3, with which we find the numerical results converge.

In Fig. 5.4, we plot the probability of the system being in the excited state $|e\rangle|1\rangle_M \otimes |0\rangle_C$ according to the numerical calculations. It is shown that the probability oscillates as a sinusoidal function. Note that the small fast oscillation patterns are due to anti-RWA effects. One can see that the larger the detuning Δ_2 is, the smaller the amplitudes of the anti-RWA patterns are. And this is understood, because larger detuning makes our approximation of eliminating the intermediate states more precise.

In order to show the improvement of the second model in Sec. 4, we plot in Fig. 5.5 the comparison between the numerical results and predictions of the two models. As is shown, the improved model results (green lines) are quite close to the numerical simulations (blue lines) in both cases, while the results of the primary model in Sec. 3 (red lines) exhibits significant errors. In particular, we compare the oscillation periods of numerical results with those theoretical prediction that $T = \pi/|\Omega_{eff}|$. It turns out that the oscillation period of the primary model has an error of about 25 percents. Hence, we see that the primary model is not accurate, though it is simple and do capture the main feature of the system. In addition, the improved model indeed makes significant progress in accuracy beyond the primary model.

Additionally, we are interested in the dependence of the oscillation on Δ_3 . As

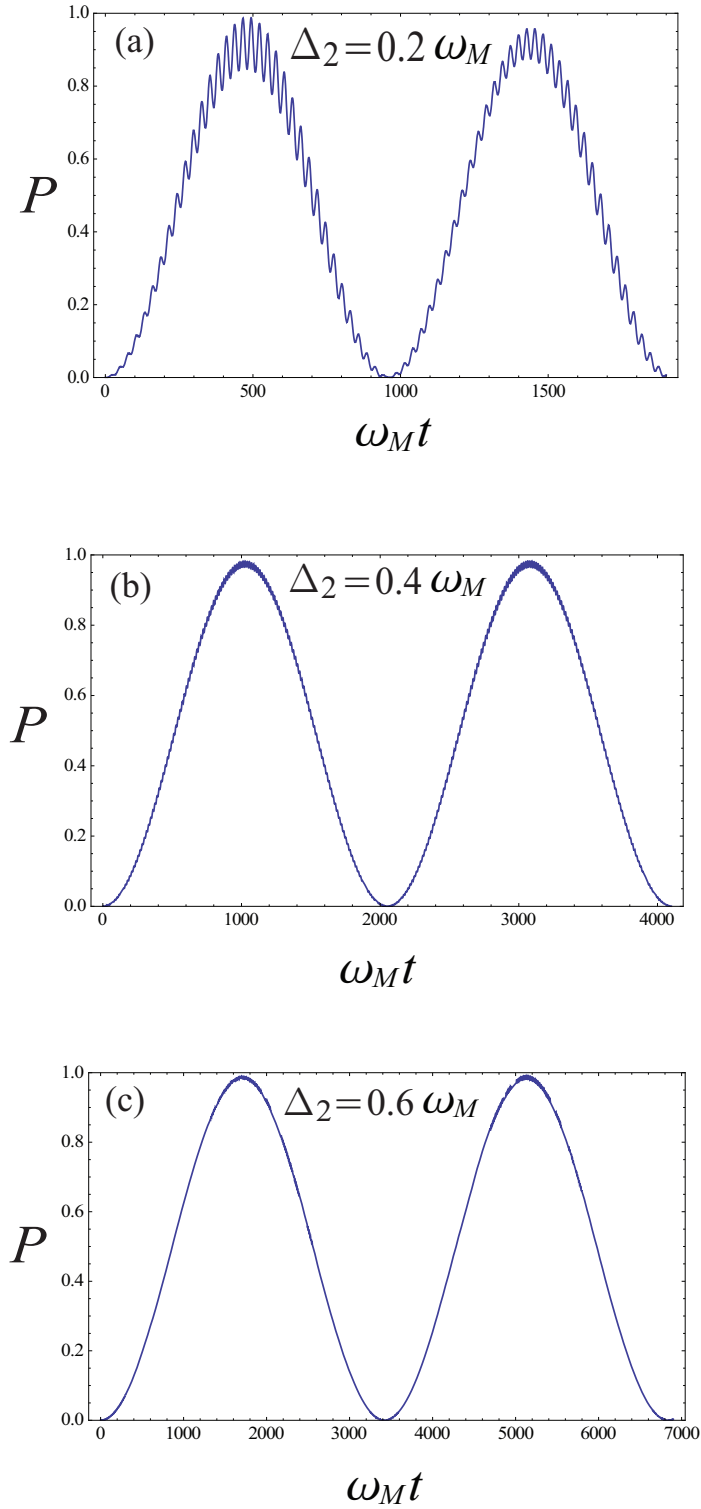


Figure 5.4: Evolution of the probability P of the system being in the state $|e\rangle|1\rangle_M \otimes |0\rangle_C$, for different detuning Δ_2 . Other parameters are: $\Delta_3 = 0$, $g = 0.4\omega_M$, $\Omega = G = 0.05\omega_M$.

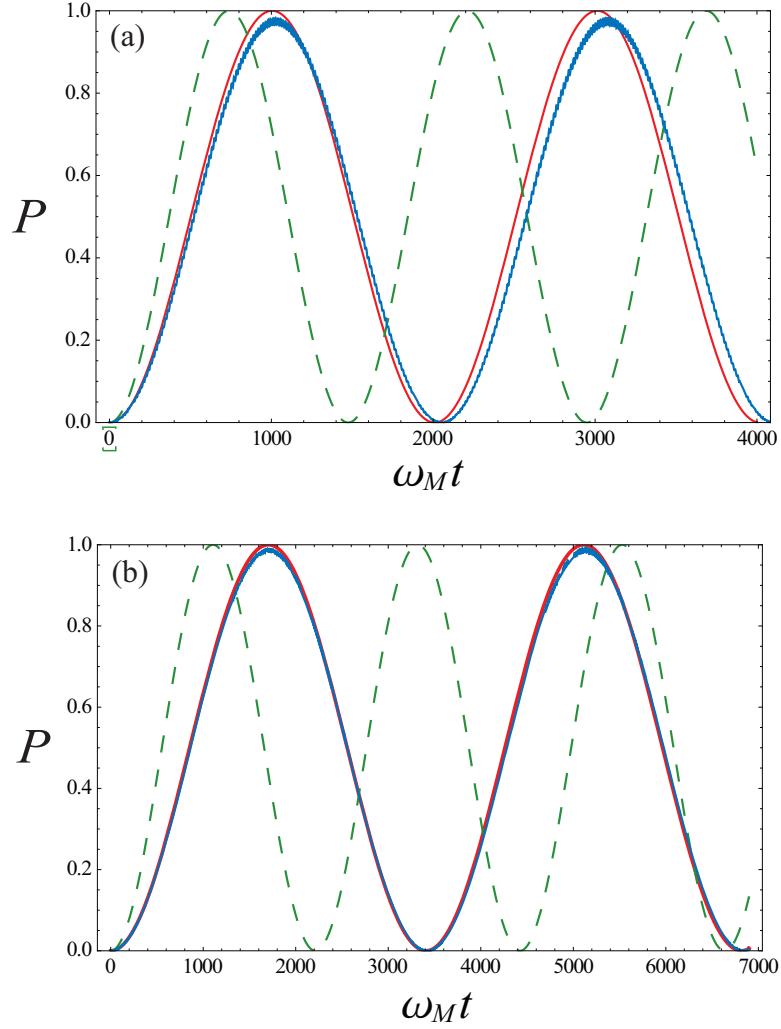


Figure 5.5: Evolution of the probability P of the system being in the state $|e\rangle|1\rangle_M \otimes |0\rangle_C$ based on the numerical simulations (blue lines), the primary model (green dashed lines) and the improved model (red lines). The parameters are: (a) $\Delta_2 = 0.4\omega_M$, (b) $\Delta_2 = 0.6\omega_M$; with the other parameters: $\Delta_3 = 0$, $g = 0.4\omega_M$, $\Omega = G = 0.05\omega_M$.

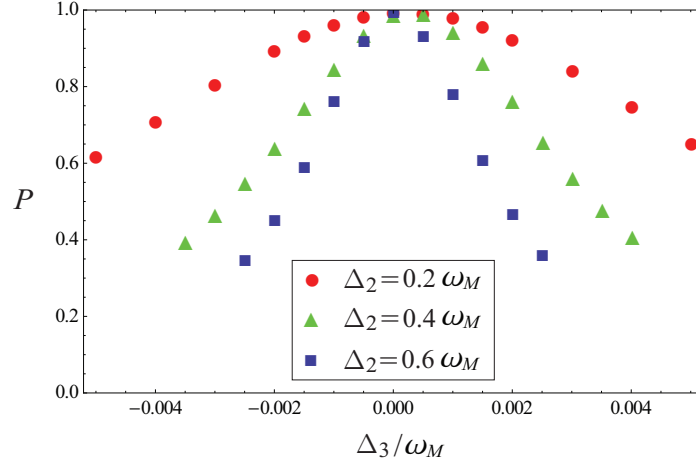


Figure 5.6: Dependence of the maximal probability P_m on Δ_3 . Other parameters are: $g = 0.4\omega_M$, $\Omega = G = 0.05\omega_M$.

is known for typical Rabi oscillations, the existence of an off-resonance detuning leads to a reduced amplitude of the oscillation. That is to say, the decrease in amplitude of the Rabi oscillation can be regarded as an indicator of its dependence on the off-resonance detuning. Therefore, we plot in Fig. 5.6 the dependence of oscillation amplitude (maximal probability in the excited state P_m) on variations of Δ_3 . It is shown that generally, the oscillation amplitudes decrease when $|\Delta_3|$ becomes larger and larger, with the peaks of the oscillation amplitudes all locating at $\Delta_3 \approx 0$, which is expected. Besides, we find that when Δ_2 is larger, the amplitude decreases faster. This is because the effective driving strength $\Omega_{eff} = -\sum_r \frac{A_{1,r}^{(1)} G A_{0,r}^{(1)} \Omega}{\varepsilon_{1,r}}$ becomes smaller with larger Δ_2 , as $\varepsilon_{1,r} = \Delta_2 + r\omega_M$. As a result, the effect of an off-resonance detuning becomes relatively more significant when Δ_2 is larger.

5.6 Effects of Damping

In this section, we quantitatively study the effects of dampings on the atom-mirror Rabi oscillations via numerical simulations based on the master equation. Gen-

erally speaking, dampings will destroy coherence of the quantum states. Hence, sufficiently low damping rates are essential to observe the Rabi oscillations.

Under Born-Markov approximation, the dissipative evolution of the whole system is governed by the following master equation:

$$\begin{aligned} \frac{d\rho}{dt} = & -i[H', \rho] - \frac{\kappa}{2} (a^\dagger a \rho - 2a \rho a^\dagger + \rho a^\dagger a) - \frac{\gamma_M}{2} (b^\dagger b \rho - 2b \rho b^\dagger + \rho b^\dagger b) \\ & - \frac{\gamma_A}{2} (\sigma_+ \sigma_- \rho - 2\sigma_- \rho \sigma_+ + \rho \sigma_+ \sigma_-), \end{aligned} \quad (5.31)$$

where κ , γ_M and γ_A are respectively, the damping rates of cavity field, mechanical motion and the atom excited state. ρ is the density matrix of the system, and H' is the Hamiltonian that governs the coherent evolution of the system given by Eq. (5.3). We have also denoted $\sigma_+ = \sigma_{eg}$ and $\sigma_- = \sigma_{ge}$ for simplicity. In addition, we assume a low temperature, such that thermal excitations of the cavity field, mechanical oscillator and the atom are zero.

First of all, we make a theoretical estimation on the magnitudes of the decay rates required in order to observe the oscillations. Generally, the population P of an excitation decays exponentially over time, i.e., $P \sim e^{-\Gamma t}$ with Γ the decay rate. To avoid significant influences from the decay, we therefore require a small decay rate satisfying $\Gamma t_0 \ll 1$ for a time period t_0 of interest, such that the decline of excitation population is insignificant. Now we apply the above general argument to our specific case of Rabi oscillations, which involve excitations of the atom and the mirror. Consequently, we require both the decay rates of the atom and mirror obey: $\gamma_A T \ll 1$ and $\gamma_M T \ll 1$. The time period of the oscillations T is roughly: $T \sim \Omega_{eff}^{-1}$, with $\Omega_{eff} \sim \Omega G / \Delta_2$. Thus, we obtain: $\gamma_A \ll \Omega G / \Delta_2$ and $\gamma_M \ll \Omega G / \Delta_2$, under which the decay effects of the atom and mirror are negligible.

On the contrary, cavity field remains in vacuum state in the Rabi oscillations, which means that ideally the damping of cavity field has no effect. However, there is always a small number of photons in the cavity that mediates the coupling between the atom and the mirror. According to the three-level model in Sec.

3, a single-photon state $|1\rangle_C |\tilde{0}\rangle_M |g\rangle$ serve as an intermediate state, which has a small occupation given by Eq. (5.12). Hence, the damping of cavity field still causes a loss of population out of the oscillating states. In particular, the net effect of cavity field damping is roughly described by an effective damping rate: $\kappa_{eff} \sim \kappa(\Omega/\Delta_2)^2$, which is the product of the original damping rate and the photon number. Therefore, the requirement for the cavity field damping rate is estimated: $\kappa \ll \Delta_2$.

Now we turn to numerical evaluations by solving the master equation (5.31) numerically with the initial state of the system being the ground state $\Psi(0) = |g\rangle |0\rangle_M \otimes |0\rangle_C$. In the calculations, we use a Hilbert space with largest photon number 2 and largest phonon number 3, with which we find the numerical results converge.

In Fig. 5.7, we provide numerical results showing the damping effects of the the two-level atom, mechanical oscillator (mirror) and cavity field, separately. In order to obtain the net effect of each damping, we always focus on one kind of damping in each figure with the other two damping rates set zero. Generally, we see that the oscillation amplitudes of the Rabi oscillations decline gradually, showing a typical feature of a damped harmonic oscillator.

In Fig. 5.7 (a), we see that an atom decay rate of $\gamma_A/\omega_M = 1 \times 10^{-4}$ causes a notable decline of oscillation amplitude to about 0.9 for the first peak. In order to show directly the leakage of probability out of the two-level states, we plot the total probability of the two state: $|g\rangle |0\rangle_M \otimes |0\rangle_C$ and $|e\rangle |1\rangle_M \otimes |0\rangle_C$ in the red line, which indeed keeps declining over time. In Fig. 5.7 (b) we see that the damping of the mirror cause a similar effect to the oscillations. Such a similarity is understood, because the dampings of the atom and mirror plays a comparable role in the master equation (5.31). In Fig. 5.7 (c), we explore the effect of cavity field damping on the atom-mirror Rabi oscillations. We find that the oscillations are much more robust against the cavity field damping than

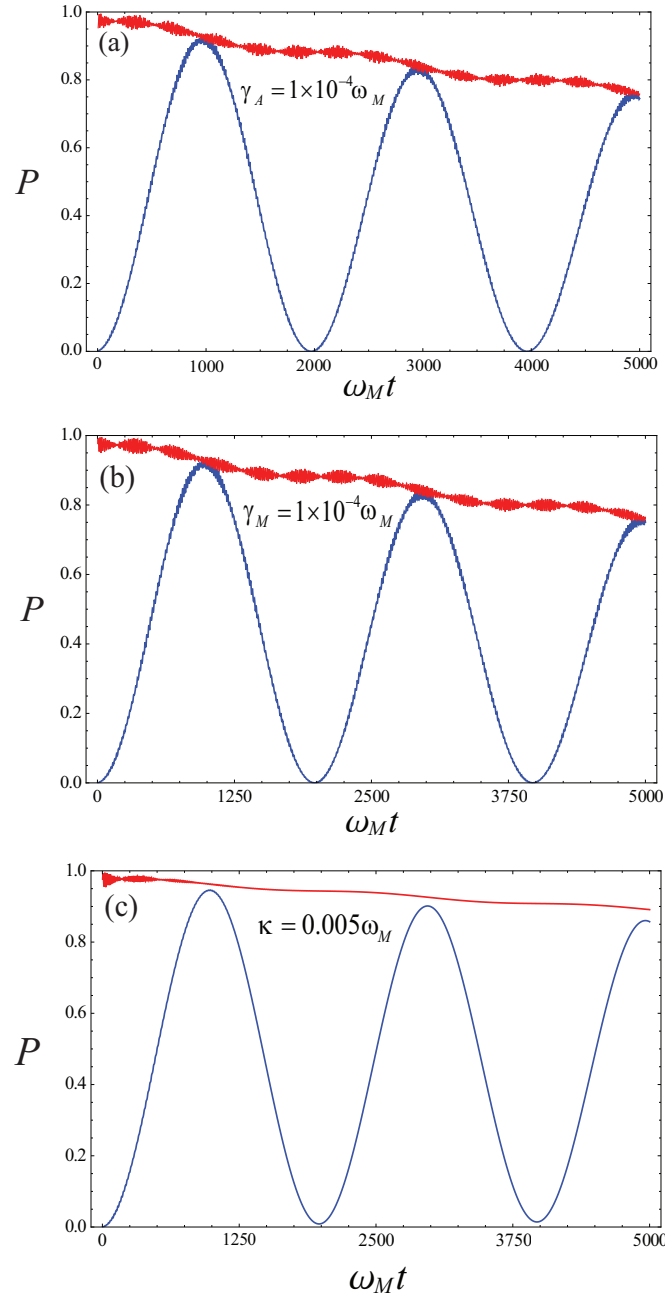


Figure 5.7: Damping effects of the atom (a), mechanical oscillator (b) and cavity field (c) on the atom-mirror Rabi oscillation. In each figure, the blue line is the probability of the system in the excited state $|g\rangle |0\rangle_M \otimes |0\rangle_C$, and red line is the total probability of being in the ground state $|g\rangle |0\rangle_M \otimes |0\rangle_C$ and the excited state $|e\rangle |1\rangle_M \otimes |0\rangle_C$. Other parameters are: $g = 0.4\omega_M$, $\Omega = G = 0.05\omega_M$, $\Delta_2 = 0.4\omega_M$.

atomic and mechanical dampings. It is shown that the oscillation amplitude still remains about 0.95 for the first peak when field damping rate κ reaches $0.005\omega_M$, which is 50 times bigger for the cases of atomic and mechanical damping. Such a result is consistent with the estimation that the cavity field damping is described by an effective damping rate: $\kappa_{eff} \sim \kappa(\Omega/\Delta_2)^2$, with the factor $(\Omega/\Delta_2)^2 \sim 10^{-2}$. Consequently, the cavity field damping rate is about two orders larger to cause a comparable influence.

5.7 Conclusion

To conclude, we have addressed an effective coupling issue between a two-level atom and a mesoscopic mirror in a driven optomechanical system with an intracavity atom in the single-photon strong coupling regime. We find that the dynamics of such a system can be described by a Λ -type three-level model under conditions of resonant laser driving [Eq. (5.15)] and weak coupling amplitudes [Eq. (5.7)]. Moreover, by eliminating the intermediate state, the three-level model further reduces to an effective two-level Hamiltonian, which leads to Rabi oscillations between two atom-mirror states with the cavity field kept in vacuum. Thus, we achieve the atom-mirror coupling effectively. Note that since the atom and mirror do not couple directly, the cavity field plays an important role as a medium of their effective coupling. Therefore, the cavity photon number is very small but can not be exactly zero during the Rabi oscillations. To support our model, we perform numerical simulations according to the Schrödinger equation governed by the exact Hamiltonian. It turns out that our model agrees well with the numerical results and the atom-mirror Rabi oscillations are observed in various cases. In addition, we quantify the influences of the atomic, mechanical and cavity field dampings via numerical simulations based on the master equation.

Chapter 6

Conclusion

In this thesis, we have addressed several quantum effects of the optomechanical coupling between a single-mode cavity field and a mechanical oscillator (harmonically bounded mirror) in the single-photon strong coupling regime theoretically. First, we have demonstrated the generation of a single photon in a driven optomechanical cavity. This is based on a two-level model involving the ground state and a single-photon state with a specific laser frequency establishing an optomechanical resonance. Such a two-level model relies on a photon blockade effect that originates from the nonlinear energy spectra of optomechanical systems. Consequently, we obtain Rabi oscillations between the ground state and a single-photon state such that the system evolves into a single-photon state at certain time, i.e., a single cavity photon is generated. In addition, such model predictions are verified by numerical calculations based on the Schrödinger equation under the exact Hamiltonian. Specifically, the near sinusoidal probability oscillation curves are observed for various sets of parameters. We also investigate the effect of cavity field damping by solving the master equation numerically and find that a cavity photon lifetime much larger than the oscillation period is essential to the successful generation of a single cavity photon.

Second, we have discovered that for an optomechanical cavity driven by two

lasers with frequencies satisfying certain resonance conditions, there exists a class of dark states that are eigenvectors of the system Hamiltonian. The dark states are superpositions of mirror number states with vacuum cavity field. When the system is in such dark states, there is no absorptions of both driving lasers, i.e., the cavity field is decoupled from the external driving. Note that such optomechanical dark states are analogous to coherent population trapping (CPT) in atomic physics with the same principle of quantum destructive interference. We provide an analytical expression of the dark states and show with numerical examples that phonon number distributions of the dark states exhibit sub-Poissonian statistics. In addition, the dark states can be prepared with high fidelities by optical pumping, which is demonstrated with numerical calculations based on the master equation.

Third, for a driven optomechanical cavity with a two-level atom inside we have achieved an effective coupling between the atom and the mesoscopic mirror. Under certain conditions, the dynamics of the whole system is captured by a Λ -type three-level Hamiltonian. Moreover, the intermediate state in such a three-level Hamiltonian can be eliminated in the large detuning limit, such that the system is described by a two-level resonant Hamiltonian involving the ground state and an atom-mirror excited state with the cavity field kept in vacuum. Such a two-level Hamiltonian leads to a Rabi oscillation in which the excitation of the atom is accompanied by the phonon excitation of the mirror, i.e., an effective coupling between the atom and the mirror is achieved. Since the atom and the mirror do not couple with each other directly in the original Hamiltonian, such an effective coupling is actually mediated by the cavity field. Notably, such Rabi oscillations are observed for various cases in numerical simulations based on the Schrödinger equation under the exact Hamiltonian. Besides, the influences of the dissipations of the atom, mirror and cavity field are quantified by numerically solving the full master equation.

Moreover, we remark that the parameters required for realizing the models in this thesis are still challenging in experiments. Specifically, we require the combined regime of single-photon strong coupling and resolved sidebands. Currently, the resolved sidebands regime has already been achieved in a number of experiments with different configurations [40, 46, 64]. However, the single-photon strong coupling regime is not reached in most experimental setups. Exceptionally, for the configuration of an optomechanical system with a cloud of ultracold atoms serving as the mechanical oscillator, the single-photon strong coupling regime has already been reached [47]. But the resolved sideband condition is not satisfied in this experiment. In order to achieve a single-photon strong coupling, the size of the optical cavity and the mass of the mechanical oscillator should be sufficiently small. At last, we believe that with the advances of techniques, our models can be experimentally verified in the future.

Bibliography

- [1] T. J. Kippenberg and K. J. Vahala, *Science* **321**, 1172 (2008).
- [2] F. Marquardt and S. M. Girvin, *Physics* **2**, 40 (2009).
- [3] I. Favero and K. Karrai, *Nat. Photonics* **3**, 201 (2009).
- [4] M. Aspelmeyer, S. Gröblacher, K. Hammerer, and N. Kiesel, *J. Opt. Soc. Am. B* **27**, A189 (2010).
- [5] P. Meystre, e-print arXiv:1210.3619.
- [6] M. Aspelmeyer, T. J. Kippenberg and F. Marquardt, e-print arXiv:1303.0733.
- [7] V. Fiore, Y. Yang, M. C. Kuzyk, R. Barbour, L. Tian, and H. Wang, *Phys. Rev. Lett.* **107**, 133601 (2011).
- [8] J. Zhang, K. Peng, and S. L. Braunstein, *Phys. Rev. A* **68**, 013808 (2003).
- [9] K. Stannigel, P. Rabl, A. S. Sørensen, P. Zoller, and M. D. Lukin, *Phys. Rev. Lett.* **105**, 220501 (2010).
- [10] S. Mancini, V. Giovannetti, D. Vitali, and P. Tombesi, *Phys. Rev. Lett.* **88**, 120401 (2002).
- [11] C. Genes, D. Vitali, and P. Tombesi, *Phys. Rev. A* **77**, 050307 (2008).

- [12] C. Genes, A. Mari, P. Tombesi, and D. Vitali, *Phys. Rev. A* **78**, 032316 (2008).
- [13] A. Ferreira, A. Guerreiro, and V. Vedral, *Phys. Rev. Lett.* **96**, 060407 (2006).
- [14] D. Vitali, S. Gigan, A. Ferreira, H. R. Böhm, P. Tombesi, A. Guerreiro, V. Vedral, A. Zeilinger, and M. Aspelmeyer, *Phys. Rev. Lett.* **98**, 030405 (2007).
- [15] M. Paternostro, D. Vitali, S. Gigan, M. S. Kim, C. Brukner, J. Eisert, and M. Aspelmeyer, *Phys. Rev. Lett.* **99**, 250401 (2007).
- [16] M. J. Hartmann and M. B. Plenio, *Phys. Rev. Lett.* **101**, 200503 (2008).
- [17] M. Bhattacharya, P.-L. Giscard, and P. Meystre, *Phys. Rev. A* **77**, 030303 (2008).
- [18] S. Bose, K. Jacobs, and P. L. Knight, *Phys. Rev. A* **56**, 4175 (1997).
- [19] W. Marshall, C. Simon, R. Penrose, and D. Bouwmeester, *Phys. Rev. Lett.* **91**, 130401 (2003).
- [20] D. Kleckner, I. Pikovski, E. Jeffrey, L. Ament, E. Eliel, J. van den Brink, and D. Bouwmeester, *New J. Phys.* **10**, 095020 (2008).
- [21] O. Romero-Isart, A. C. Pflanzer, F. Blaser, R. Kaltenbaek, N. Kiesel, M. Aspelmeyer, and J. I. Cirac, *Phys. Rev. Lett.* **107**, 020405 (2011).
- [22] I. Pikovski, M. R. Vanner, M. Aspelmeyer, M. S. Kim, and C. Brukner, *Nat. Phys.* **8**, 393 (2012).
- [23] V. B. Braginsky, and A. B. Manukin, *Sov. Phys. JETP* **25**, 653 (1967).
- [24] J. D. Thompson, B. M. Zwickl, A. M. Jayich, F. Marquardt, S. M. Girvin, and J. G. E. Harris, *Nature (London)* **452**, 72 (2008).

- [25] J. C. Sankey, C. Yang, B. M. Zwickl, A. M. Jayich and J. G. E. Harris, *Nat. Phys.* **6**, 707-712 (2010).
- [26] P. Verlot, A. Tavernarakis, T. Briant, P.-F. Cohadon, and A. Heidmann, *Phys. Rev. Lett.* **102**, 103601 (2009).
- [27] G. S. Agarwal and S. Huang, *Phys. Rev. A* **81**, 041803(R) (2010).
- [28] S. Huang and G. S. Agarwal, *Phys. Rev. A* **83**, 043826 (2011).
- [29] H. Xiong, L. G. Si, A. S. Zheng, X. Yang, and Y. Wu, *Phys. Rev. A* **86**, 013815 (2012).
- [30] S. Weis, R. Rivière, S. Deléglise, E. Gavartin, O. Arcizet, A. Schliesser, T. J. Kippenberg, *Science* **330**, 1520 (2010).
- [31] A. H. Safavi-Naeini, T. P. Mayer Alegre, J. Chan, M. Eichenfield, M. Winger, Q. Lin, J. T. Hill, D. E. Chang and O. Painter, *Nature (London)* **472**, 69 (2011).
- [32] M. Karuza, C. Biancofiore, C. Molinelli, M. Galassi, R. Natali, P. Tombesi, G. Di Giuseppe, and D. Vitali, e-print arXiv:1209.1352.
- [33] C. Dong, V. Fiore, M. C. Kuzyk, H. Wang, *Science*, **338**, 1609 (2012).
- [34] A. Schliesser, and T. J. Kippenberg, *Advances in atomic, molecular and optical physics (Elsevier Academic Press)* (2010).
- [35] M. Ludwig, B. Kubala, and F. Marquardt, *New J. Phys.* **10**, 95013 (2008).
- [36] C. Fabre, M. Pinard, S. Bourzeix, A. Heidmann, E. Giacobino, and S. Reynaud, *Phys. Rev. A* **49**, 1337 (1994).
- [37] A. Mari and J. Eisert, *Phys. Rev. Lett.* **103**, 213603 (2009).
- [38] J.-Q. Liao and C. K. Law, *Phys. Rev. A* **83**, 033820 (2011).

- [39] M. Eichenfield, J. Chan, R. M. Camacho, K. J. Vahala, and O. Painter, *Nature (London)* **462**, 78 (2009).
- [40] J. Chan, T. P. M. Alegre, A. H. Safavi-Naeini, J. T. Hill, A. Krause, S. Gröblacher, M. Aspelmeyer, O. Painter, *Nature (London)* **478**, 89 (2011).
- [41] J. Chan, A. H. Safavi-Naeini, J. T. Hill, S. Meenehan, O. Painter, *Appl. Phys. Lett.* **101**, 081115 (2012)
- [42] M. Davanço, J. Chan, A. H. Safavi-Naeini, O. Painter, K. Srinivasan, e-print arXiv: 1207.5020
- [43] L. Ding, C. Baker, P. Senellart, A. Lemaitre, S. Ducci, G. Leo, and I. Favero, *Appl. Phys. Lett.* **98**, 113108 (2011)
- [44] J. D. Teufel, D. Li, M. S. Allman, K. Cicak, A. J. Sirois, J. D. Whittaker, R. W. Simmonds, *Nature (London)* **471**, 204 (2011)
- [45] A. Xuereb, C. Genes, and A. Dantan, *Phys. Rev. Lett.* **109**, 223601 (2012)
- [46] E. Verhagen, S. Deléglise, S. Weis, A. Schliesser, T. J. Kippenberg, *Nature (London)* **482**, 63 (2012)
- [47] K. W. Murch, K. L. Moore, S. Gupta, and D. M. Stamper-Kurn, *Nature Phys.* **4**, 561 (2008).
- [48] P. Rabl, *Phys. Rev. Lett.* **107**, 063601 (2011).
- [49] J. Qian, A. A. Clerk, K. Hammerer, and F. Marquardt, *Phys. Rev. Lett* **109**, 253601 (2012).
- [50] A. Nunnenkamp, K. Børkje, and S. M. Girvin, *Phys. Rev. Lett.* **107**, 063602 (2011).
- [51] A. Kronwald, M. Ludwig, F. Marquardt, *Phys. Rev. A* **87**, 013847 (2013).

- [52] D. Kleckner, B. Pepper, E. Jeffrey, P. Sonin, S. M. Thon, and D. Bouwmeester, *Opt. Express* **19**, 19708 (2011).
- [53] B. D. Cuthbertson, M. E. Tobar, N. Ivanov E, and D. G. Blair, *Rev. Sci. Inst.* **67**, 2435 (1996).
- [54] S. Gröblacher, K. Hammerer, M. R. Vanner, and M. Aspelmeyer, *Nature (London)* **460**, 724 (2009)
- [55] O. Arcizet, C. Molinelli, P.-F. Briant T. anf Cohadon, A. Heidmann, J.-M. Mackowksi, C. Michel, L. Pinard, O. Francais, and L. Rousseau, *New J. Phys.* **10**, 125021 (2008).
- [56] B. He, *Phys. Rev. A* **85**, 063820 (2012).
- [57] K. J. Vahala, *Nature (London)* **424**, 839 (2003).
- [58] H. K. Cheung and C. K. Law, *Phys. Rev. A* **84**, 023812 (2011).
- [59] C. K. Law, *Phys. Rev. A* **51**, 2537 (1995).
- [60] J. Q. Liao, H. K. Cheung, and C. K. Law, *Phys. Rev. A* **85**, 025803 (2012).
- [61] M. Paternostro, D. Vitali, S. Gigan, M. S. Kim, C. Brukner, J. Eisert, and M. Aspelmeyer, *Phys. Rev. Lett.* **99**, 250401 (2007)
- [62] T. Botter, D. W. C. Brooks, N. Brahms, S. Schreppler, and D. M. Stamper-Kurn, *Phys. Rev. A* **85**, 013812 (2012).
- [63] P. Tombesi, S. Gigan, and M. Aspelmeyer, *Phys. Rev. A* **77**, 33804 (2008).
- [64] J. Teufel, T. Donner, Dale Li, J. W. Harlow, M. S. Allman, K. Cicak, A. J. Sirois, J. D. Whittaker, K.W. Lehnert, and R.W. Simmonds, *Nature (London)* **475**, 359 (2011).

- [65] A. A. Clerk, M. H. Devoret, S. M. Girvin, F. Marquardt, and R. J. Schoelkopf, *Rev. Mod. Phys.* **82**, 1155 (2010).
- [66] C. W. Gardiner and P. Zoller, *Quantum Noise*, Springer, Berlin, 3rd edition, 2004
- [67] P. Kómár, S. D. Bennett, K. Stannigel, S. J. M. Habraken, P. Rabl, P. Zoller, and M. D. Lukin, e-print arXiv:1210.4039.
- [68] A. Nunnenkamp, K. Børkje, and S. M. Girvin, *Phys. Rev. A* **85**, 051803(R) (2012).
- [69] W. H. Louisell, *Quantum statistical properties of radiation*, John Wiley & Sons, 1973.
- [70] J. Q. Liao, and C. K. Law, *Phys. Rev. A* **84**, 053838 (2011).
- [71] K. Stannigel, P. Komar, S. J. M. Habraken, S. D. Bennett, M. D. Lukin, P. Zoller, and P. Rabl, *Phys. Rev. Lett.* **109**, 013603 (2012).
- [72] F. A. M. de Oliveira, M. S. Kim, P. L. Knight, and V. Buek, *Phys. Rev. A* **41**, 2645 (1990).
- [73] Y.-D. Wang and A. A. Clerk, *Phys. Rev. Lett.* **108**, 153603 (2012).
- [74] Y.-D. Wang and A. A. Clerk, *New J. Phys.* **14**, 105010 (2012).
- [75] J. Q. Liao and C. K. Law, *Phys. Rev. A* **87**, 043809 (2013).
- [76] C. Soller et al., *Phys. Rev. A* **83**, 031806(R) (2011).
- [77] K. Jähne, C. Genes, K. Hammerer, M. Wallquist, E. S. Polzik and P. Zoller, *Phys. Rev. A* **79**, 063819 (2009).
- [78] C. A. Regal, J. D. Teufel, and K. W. Lehnert, *Nature Phys.* **4**, 555 (2008).

- [79] A. Nunnenkamp, K. Børkje, J. G. E. Harris, and S. M. Girvin, *Phys. Rev. A* **82**, 021806(R) (2010).
- [80] E. Arimondo, *Prog. Optics*, **35**, 257, (1996).
- [81] H. R. Gray, R. M. Whitley, and C. R. Stroud, Jr., *Opt. Lett.*, **3**, 218 (1978).
- [82] S. E. Harris, J. E. Field, and A. Imamoglu, *Phys. Rev. Lett.* **64**, 1107 (1990).
- [83] G. Alzetta, A. Gozzini, L. Moi and G. Orriols, *Nuovo Cimento* **36B**, 5(1976).
- [84] M. Fleischhauer, A. Imamoglu and J. P. Marangos, *Rev. Mod. Phys.*, Vol. **77**, No. 2 (2005).
- [85] J. P. Marangos, *J. Mod. Optics.*, Vol. **45**, No. 3, (1998).
- [86] G.-F. Xu and C. K. Law, *Phys. Rev. A* **87**, 053849 (2013).
- [87] L. Tian, *Phys. Rev. Lett.* **108**, 153604 (2012).
- [88] M. Ludwig, A. H. Safavi-Naeini, O. Painter, and F. Marquardt, *Phys. Rev. Lett.* **109**, 063601 (2012).
- [89] S. Singh, H. Jing, E. M. Wright, and P. Meystre, *Phys. Rev. A* **86**, 021801(R) (2012).
- [90] F. Khalili, S. Danilishin, H. Miao, H. Müller-Ebhardt, H. Yang, and Y. Chen, *Phys. Rev. Lett.* **105**, 070403 (2010).
- [91] L. Tian, and H. Wang, *Phys. Rev. A* **82**, 053806 (2010).
- [92] K. Hammerer, M. Wallquist, C. Genes, M. Ludwig, F. Marquardt, P. Treutlein, *Phys. Rev. Lett.* **103**, 063005 (2009).